THE GRAVITY FIELD AND CRUSTAL STRUCTURE OF THE SOUTHERN END OF THE ETHIOPIAN RIFT SYSTEM

By

Alemayehu Lakew

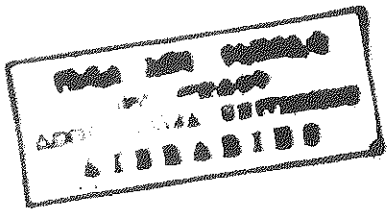

A Thesis

submitted to the

School of Graduate Studies

Addis Ababa University

In Partial Fulfilment of

the Requirements of the Degree

Master of Science in Physics

June 1993

Dedicated

TO

The memory of my mother

Tiru Amognei

TABLE OF CONTENTS

ACKNOWLEDGEMENTS

I have no words to say about my supervisor **Dr. Abera Alemu**, he is my brother, friend, and teacher. He did many things to me that no one can do, even my relatives. I have really benefited from his publications and his unfailing effort, talent in the field, and computer usage to bring this thesis its present final stage. Directly or indirectly he was guiding me to the right paths of both the academic and social lives. Now, I feel self confident to do research on my own in gravity (geophysics) with little or no assistance if I am given the chance. My second acknowledgement goes to his wife, **Architect Birke Yami**, who helped me much in drafting the Bouguer anomaly map and preparing the figures cited in the thesis.

I would like to acknowledge my co-supervisor **Ato Mulugeta Alene** for his valuable comments and suggestions, especially on the geological back ground of the thesis.

I respect and acknowledge **Dr. Tilahun Mamo** who pushed me in the field of geophysics since the time of my attendance in his lectures of the course entitled "Advanced Geophysics". I would have not been doing this thesis without his effort in finding a supervisor, it was through him that I came to be attached with Dr. Abera Alemu.

Let God bless my wife **Menbere Ejigu** and my little lovely daughter and sister **Biruh Alemayehu** without whom I could not be successful. It is their patience that brought the end of those

hard times peacefully.

I can not forget my friend and brother **Yohannes G/Eyesus**, who faced with me the troubles of my undergraduate University life. It was his brotherly advice and material support that I came to be born in the world of intellectuals. I also thank his sisters and brothers for their encouragement and brotherhood approach.

My sister **Selam Melese** is thanked for her material and moral support during my undergraduate life.

The last but not least, I say thanks to the staff of the Geophysical observatory of, AAU, especially **Ato Dagmawi Shiferaw** who showed me the ABC of using a computer. I also thank **Dr. Laike Mariam Assfaw** who allowed me to use the facilities of the Geophysical Observatory.

The **School of Graduate Studies** is duly acknowledged for funding the research.

LIST OF FIGURES

LIST OF TABLES

ABSTRACT

The Bouguer anomaly map of the rift zone south of the southern end of the Main Ethiopian rift between Lat. 4^0 00'N - 7^0 00'N and Long. 36^0 00'E - 39^0 45'E is presented. The computed Bouguer anomaly map shows a complex pattern of positive and negative Bouguer gravity anomalies. A positive Bouguer gravity anomaly of -165 mGal occurs over the floor of the Abaya-Chamo rift and is flanked by negative anomalies that reside on its shoulders. The anomaly pattern associated with the Chew Bahir rift is completely different from the other regions. The floor has a negative gravity anomaly of magnitude -135 mGal and is flanked by positive gravity anomalies residing on its shoulders. This may be attributed to the swamp and volcano-lacostrine nature of the rift floor. Further south in Kenya, the Bouguer anomaly map shows that there is a relative increase in magnitude of the regional gravity field with a complex pattern of alternating positive and negative anomalies which are generally oriented a NNW-SSE and E-W direction.

Two profiles that run through the major tectonic systems (the Abaya-chamo rift and the Chew Bahir rift) of interest in the area were extracted from the Bouguer anomaly map. 2½-D gravity models were constructed along these profiles. The results of the model calculations are that:

Along Profile AA, the crust beneath the plateaus is 35 to 40 km thick. Within the axis of the Abaya-Chamo rift the crust thins to 29 km. Along profile BB, the crust beneath the high lands in the vicinity of the Amaro horst is 35 to 40 km thick. Beneath

the rift zone, i.e., the floor of the Chew Bahir rift and the flanking uplifted regions the crust thins to 27 km. The observed crustal thinning beneath the rift zones along both profiles is thought to be caused by an upward progression of low density mantle material (anomalous mantle) that intrudes itself into the lower crust.

CHAPTER 1: INTRODUCTION

Ethiopia is identified with three physiographic regions: the Western plateau, the Ethiopian Rift system and the Eastern plateau. The Ethiopian Rift system has three sectors: the Afar Depression, the Main Ethiopian Rift (MER) and the Rift system of Southern Ethiopia (Moore and Davidson, 1978). The rift system forms one of the major continental rift valleys. Almost all earthquakes and recent volcanic activities in Ethiopia are visibly associated with the rift structure and parts of the plateaus. On the other hand, there are no satisfactory geodynamic models that can explain these and other related phenomena. The lack of sound geodynamic concept inturn hampers the understanding of the causes of earthquakes, volcanic activities, mineral exploration and energy resources development in continental rift systems like that of the Ethiopian Rift system. Thus, this research is concerned with the contribution of gravimetric solutions to these problems by collecting gravity data within a 130,000 km^2 study area. The investigated area covers the region between the southern sector of the MER and the northern sector of Turkana rift of northern Kenya (Lat. 3^0 00'N - 7^0 00'N and Long. 36^0 00'E-39^0 45'E).

The main objectives of this thesis are:

To fill the gap in the regional gravity coverage between the northern part of the Kenyan Rift and the southern part of the Main Ethiopian Rift, with the aim of presenting reliable

gravity data for the region. As the region is almost void of gravity measurements, it is believed that this data will form a sound basis for further investigating the crustal structure of the region. Apart from filling the gap in the regional gravity coverage, it is hoped that the data would fulfil two specific objectives: first, the establishment of the regional gravity field over East Africa necessary for the interpretation of the large negative anomaly associated with the East African rift system (Girdler et al., 1969) and secondly, the investigation of the distribution (appearance) of the positive and negative gravity anomalies in the study area and make a comparison with the distribution of the gravity anomalies found in the Afar Depression (Makris et al., 1972; Makris et al., 1975), the MER (Alemu, 1983, 1988, 1992, Alemu & Sjöberg, 1990) and the Kenyan rift (Searle and Gouin, 1972; Swain and Khan, 1977).

To generate crustal models that produce gravity anomalies matching the observed gravity data, other previously observed geophysical data as well as the major geological and tectonic features of the region.

The present study examines regional gravity anomalies of the study area as an aid in determining the origin and nature of the various geological features present in the region.

In order to obtain a better understanding of the sources of the gravity field in the region, 2½-D crustal density models were

constructed along two profiles (Fig.9 & 10) that cross important structures. The objective is to obtain crustal models whose gravity effect possessed the same anomaly shapes and magnitudes as the observed profiles. The densities used were constrained by the results of deep seismic refraction sounding profiles in central and northern Kenya.

The Bouguer anomaly map is compiled from gravity data collected by the author and his supervisor (about 862) and the rest collected by C.Ebinger (1992), Marsden (unpublished), Kenyan gravity catalogue (Swain and Khan (1977)), and the Ethiopian Geological Survey (EIGS) (unpublished).

This thesis is organized in six chapters. The first chapter is introduction to the thesis. The second chapter discusses the geological and structural descriptions of the study area and the adjacent regions. The third chapter addresses the theoretical basis of gravity study. In the forth chapter, a discussion on the field work, data reduction, assessment of the associated errors, compilation of the Bouguer anomaly map and a qualitative description of the observed Bouguer anomalies is presented. The fifth chapter presents a quantitative description of the observed anomalies, i.e, interpretation of the gravity anomalies in terms of crustal models. In the sixth chapter, discussion, conclusions and suggestions of the study is presented. At last references cited in the thesis are presented.

CHAPTER 2: THE MAIN GEOMORPHOLOGIC AND GEOLOGIC FEATURES OF EAST AFRICA AND THE HORN OF AFRICA

2.1 GEOMORPHOLOGY OF EAST AFRICA AND THE HORN OF AFRICA

The East African system (Fig.1) may be considered to be a consequence of movements along the boundaries of three plates, viz: the Arabian, Nubian and Somalian plates. To large extent the boundary between the Arabian and the Somalian plates is the Gulf of Aden, the boundary between the Arabian and Nubian Plates is the Read Sea and the boundary between the Nubian and Somalian Plates is the rift in Ethiopia, Kenya and Tanzania (Girdler et al., 1969).

The physiographies of the Horn of Africa (Ethiopia-Somalia) and East Africa (Kenya-Uganda-Tanzania) are rather different. In the Horn a single rift valley transects the Ethiopian dome, separating the Ethiopian plateau to the west from the Somalian plateau to the east. By contrast, the East African plateau, whose 1,500 km x 1,000 km extent is virtually the same as that of the Ethiopian dome, is fringed by the western and eastern rifts of East Africa, the intervening plateau region being occupied by the shallow Lake Victoria.

The long history and large magnitude of uplift of the Ethiopian dome have resulted in deep dissection of the plateaus; for example, the Abbay (Blue Nile) River has cut a canyon 1,400 m deep in the plateau. The East African plateau is less

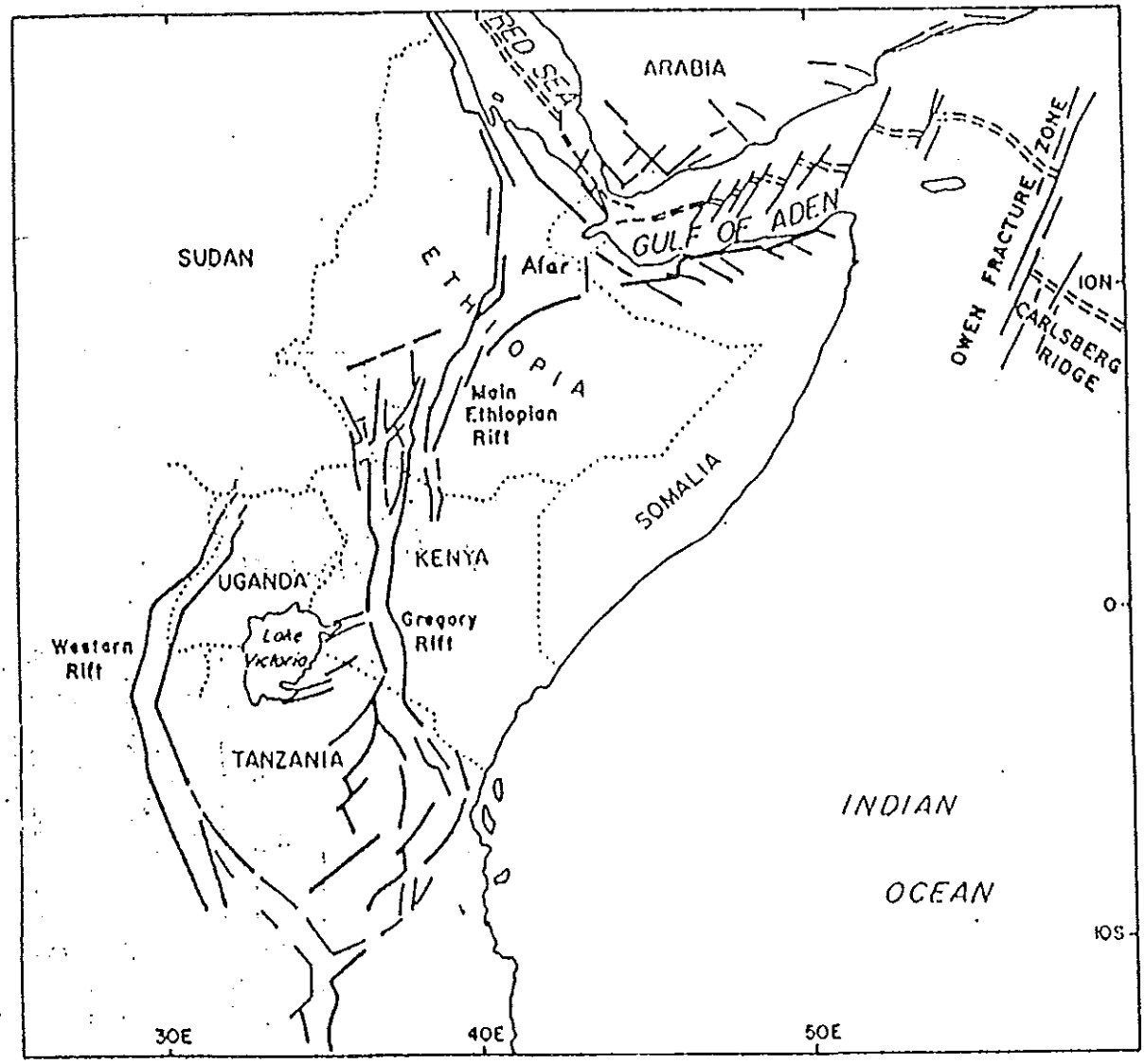

Fig. 1. The rift system in east and northeast Africa (modified from Falcon and Baker et al., 1972).

dissected, particularly in the interior region between the Eastern and Western rifts of East Africa. The greater degree of dissection of the plateaus and some of the rift margins in Ethiopia, compared with Kenya, reflects the earlier initiation of the Ethiopian uplift and associated volcanism. The elevation of the rift floor is highest in the central parts of both the Kenyan and Ethiopian domes (2,000m in Kenya, 1,700 m in Ethiopia) and declines to the fringes (600 m in south Kenya, 400 m at Lake Rudolf).

The upwarping of the plateau margins overlooking the rift valleys means that relatively little drainage enters the rifts. Thus, erosion is not a significant process on the rift floor, which is typically relatively flat due to volcanic and lacustrine accumulation. Broad transverse arches and volcanic ranges tend to separate the rift floor into a number of isolated internal drainage basins, and many of the resulting lakes are brackish or even strongly alkaline. The distinctive physiography of Afar is related to the convergence here of the Red Sea, Gulf of Aden and East African rifts (Fig.1). Excluding the influence of recent volcanism and tectonism, the floor of Afar is planar and declines from about 1,000 m in the south to -120 m at the northern apex. The Afar depression is separated from the Red Sea by the Danakil horst, which rises to 900 m (excepting volcanic cones), and from the Gulf of Aden by the Aisha horst.

The highest summits in both Kenya and Ethiopia are formed by

volcanoes which show a tendency to be situated 100 to 150 km either east or west of the eastern rift.

2.2 RIFT FORMATION IN EAST AFRICA

The causes which gave rise to the formation of the East African Rift system are hardly known. Amongst the various hypotheses are the following:

The tensional hypothesis of Gregory (1921) presumes that stretching apart of the lithosphere caused a downfaulted strip to fall between parallel normal faults. Normal faults are the commonest type of displacements observed in the rift system. However, such normal faulting cannot easily explain the irregular occurrences of the post faulting lavas, nor the fact that the edges of the plateaux bordering the rift valleys are frequently upwarped. The causes of possible tension in the lithosphere have been variously ascribed to expansion of a warming Earth, phase changes within the upper mantle, and to continental drift of eastern Africa and Arabia north-eastwards being accompanied by frictional drag and disruption.

The compressional hypothesis of Wayland (1933) can account for the uplift of the huge Ruwenzori horst in the western rift, the irregular occurrence of the lavas (strong compressional faulting would tend to "bottle down" the magmas), and the observed negative anomalies over the African Rift system south of Afar. Unfortunately for this hypothesis, proven thrust

faults are decidedly rare, the major faults being invariably normal ones.

Therefore, the rift system seems to be the result of fracturing of the lithosphere under tension, the fractured blocks being free to move under isostatic readjustment forces. The causes of tension in the case of the African Rift system was undoubtedly related to the uplift of the swells, large swells being associated with well-formed rift and vice-versa (Mohr, 1971a).

2.3 STRUCTURE OF THE ETHIOPIAN RIFT SYSTEM

The Ethiopian rift is a 1000 km long structure running NNE-ward from the Kenyan boarder to central Afar and possibly to the Red sea coast (Fig. 1). It can be divided into distinct sectors separated by tectonic/topographic discontinuities. They are, from north to south:

The Afar Depression

The Main Ethiopian Rift

The Southern Ethiopian Rift

2.3.1 THE AFAR DEPRESSION

The Afar depression occupies the area of junction of the East African, Red Sea, and Gulf of Aden rifts (Mohr, 1967a, 1987)

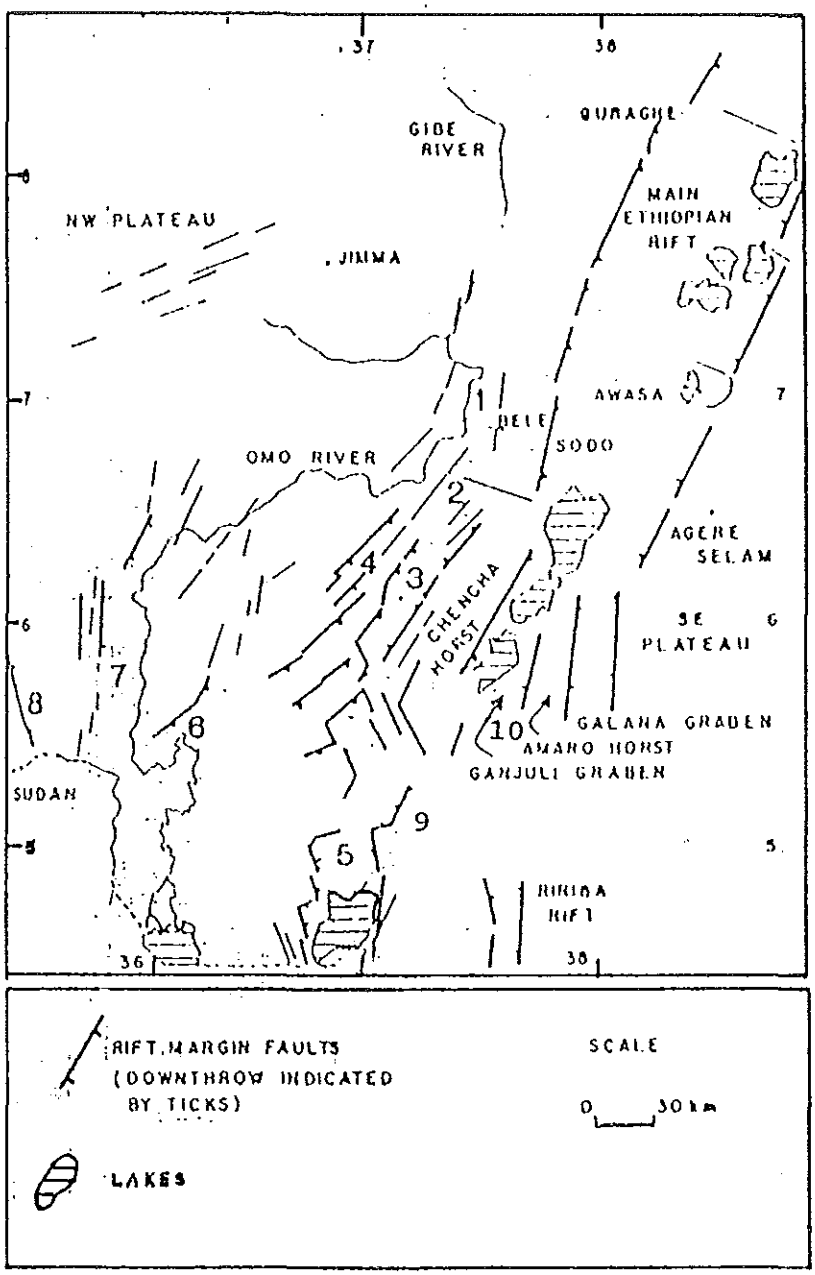

Fig. 2: Southern sector of Main Ethiopian Rift and adjacent rift zones. 1-Omo Canyon abandond rift; 2-Maze basin; 3-Bala rift; 4-Gofa basin and range; 5-Chew Bahir (Stefania) rift; 6-Usno rift; 7-Omo rift; 8-Kibish rift; 9-Boran Uplift; 10-Konso Upland.

(Fig.1) Afar is almost completely surrounded by continental crustal blocks: to the west the Ethiopian Plateau; to the south the Somalian plateau; to the east the Aisha (Ali Sabiet) horst; and to the north the Danakil horst. Mesozoic marine sediments and early Tertiary Trap series basalts of the Ethiopian and Somalian plateaus dip and thicken toward the southern and central parts of the Afar depression, dips increasing with depth in the succession (Jepsen and Athearn, 1961).

A variety of structures trend perpendicular to the margins of the Afar depression, including normal faults, tight monoclines, basalt dike swarms, and even mild compressional folds ranging from Jurassic to Quaternary in age. The floor of the depression is dominated by sub-parallel belts of closely spaced mid-Pleistocene faults, which tend to persist over long distances and reach densities of two or three faults per kilometre. Horst and graben patterns occur, but, as in the Wonji fault belt, the structure is commonly antithetic. The fault throws rarely exceed 100 m and in some areas they are associated with gaping fissures. The fault belts tend to be oriented parallel to the nearest margin of Afar, but there are many deviations, in particular south of Lake Julietti and in the annular fault Zones of northeast Afar and the Lake Abbe region.

2.3.2 THE MAIN ETHIOPIAN RIFT

This rift is divided into four separate sectors:

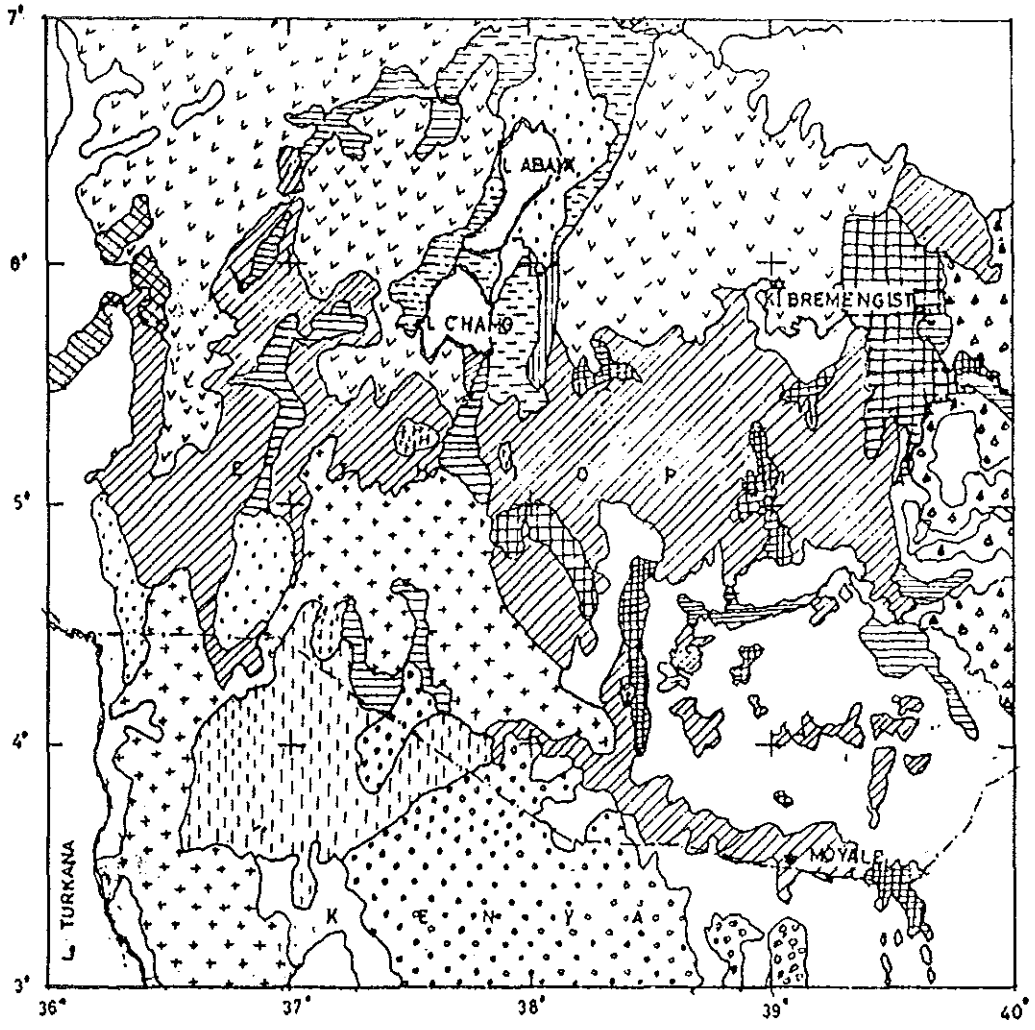

High-grade metamorphic: granitic and feldspathic gneiss; biotite and amphibole gneiss; rare granulites;migmatites; amphibolites; quartzites. (precambrian: upper proterozoic)

Lacustrine and swamp deposits; volcano lacustrine deposits of the rift floor.(pleistocene to present)

Alluvial deposits. (pleistocene to present)

Eluvial and Colluvial deposits, talus, sheet floods, dunes and beach deposits. (pleistocene to present)

Turkana-Teltale fissural basalts. (Oligocene to Miocene)

Fissural basalts. (Pliocene)

Basalts, mainly fissural. (Quaternary)

Jima volcanics: abundant rhyolities and trachy basalts. (Oligocene to Miocene)

Ignimbrites and pumices of the rift floor and subord, lacustrine deposites. (Pliocene)

Adigrat sand stones: Variegated, quartzose sand stones, of fluvial and/or littoral origin. (Trias to dogger)

Rhyolites in thick sheets and domes. (Pliocene)

Granites and quartz-diorites. (Lower palaeozoic and Precambrian)

Hamanler and iscia Baidoa formations: organogenic and olitic limestones (Callovian to oxfordian)

Fig3. Geology map of the study area (southern part of Ethiopia). (adapted from the "Geologic Map of Ethiopia and Somalia" (Merla et al, 1973.)

The northern sector: Extends from Dofani volcano south to the Awash-Meki watershed.

The Central Lakes sector: Encompasses the region of internal drainage between the Awash-Meki watershed in the north and the Awasa volcanotectonic basin in the south.

The Billati basin sector: Occurs to west and south of the central lakes sector, and controls the southward course of the Billati river system. The southern limit of this sector is drawn at the latitude of the northern shores of Lake Abaya.

The southern sector: Extends from Lake Abaya south to the middle Sagan valley. This sector of the rift is bifurcated by the Amaro horst into two branches, the Ruspoli (Lake Chamo) graben on the west and the Galana graben to the east (Fig. 2). The Amaro horst, formed of precambrian gneiss and Tertiary volcanics rising 2 km above the neighbouring grabens, shows evidence of repeated uplifts, mainly on its eastern step-faulted side, giving it a west ward dip slope. The 35 km wide Ruspoli graben to the west of the horst contains an axial swarm of young faults which continues with varying intensity along the entire length of the main Ethiopian rift floor and is known as the Wonji fault belt (Mohr, 1960).

2.3.3 RIFT STRUCTURE IN SOUTHERN ETHIOPIA

In southern Ethiopia the East African rift zone occupies a width of at least 300 km (Moore and Davidson, 1978). Figure 2 depicts the fault pattern of the southern Ethiopian Rift. The region shows extremely varied topography; elevations range from 3568 m a.s.l. in the Gemu highland to 375m a.s.l. at Lake Rudolf. There is close correlation between topography and rifting in all but the northwestern part of the region. It includes three major rift valleys and a basin- and- range terrain, from east to west: Ririba, Chew Bahir (Stefanie), the Gofa basin and-range province, and the Turkana (Lake Rudolf) (Fig. 2). The Main Ethiopian Rift is a pronounced feature in the vicinity of Lake Chamo. Southwards, it disappears in the Konso upland north of Sagan River. The Ririba Rift is a shallow feature, but with important associated Quaternary volcanism; it lies south of, and on strike with, the Amaro Horst (Levitte et al.,1974), which is immediately east of Lake Chamo. The Ririba Rift is separated from the Stefanie Rift by the Boran uplift of Tertiary volcanic rocks (Fig. 3)

The Chew Bahir (Stefanie) rift has serrated margins on both east and west sides along faults that yield steep walls up to 1500m high. Northwards, this graben is interrupted successively by the Woyto Horst and by the Gofa basin-and-range province (Fig. 2), a gently arcuate system of predominantly northeast-trending blocks tilted towards the northwest. West of the Chew Bahir rift is the Hamer Horst, a huge tilted basement block,

the surface of which dips to the west-southwest beneath a veneer of basalt and the pliocene to recent beds of the Lake Rudolf-Lower Omo River depression. The basin-and-range province culminates in the Ari highland to the north; its expression diminishes in both directions along strike. The full length of the Chew Bahir rift is underlain by a complete early lava sequence on top of the precambrian crystalline basement, a sequence that includes Eocene, Oligocene and Miocene lavas capped by pliocene lavas and sediments (Davidson, 1983) (Fig. 3). The southern part of the Chew Bahir rift, which is characterized by pleistocene-Holocene eruption and faulting, is on line with the northern extension of the axial graben of the Gregory rift (Baker et al.,1972; Mohr & Wood,1976; Moore & Davidson, 1978).

Regional geological arguments suggest that Chew Bahir rift is in a young stage of abandonment, as the north-northeast-south-southwest MER propagates into the Ririban rift region between the Ethiopian and Kenyan domes (Wolde Gabriel, and Aronson, 1987). The Turkana (Lake Rudolf) rift is a broad half-graben, broken into two branches northwards by the Nkalabong Horst, a west-tilted block of sialic lavas and tuffs mantled by the Pliocene Mursi basalt (De Heinzelin et al.,1971). The rift is bounded sharply on the west by major north-and northeast-striking faults along the east sides of the Ilibai Horst and the Shasha complex. Within the Lake Rudolf graben, beds of the Plio-Pleistocene Omo Group (De Heinzelin et al.,1971) (Fig. 2 & 3) have been broken by numerous minor faults with similar

orientations. Strong linear trends in the lower Omo and Usno Rivers are probably related to the strike of west-tilted block, rather than being localized by faults.

2.4 VOLCANISM

Volcanism in East Africa commenced with explosive activity at early Miocene nephelinite volcanoes, mainly in the Kenya-Uganda border region. After the first phase of rift faulting, which was mid-Miocene in Afar but early Pliocene in Kenya and south-central Ethiopia, volcanic activity was largely confined to the rift floor and margins. In Ethiopia, the earliest basalts of the Pliocene-Quaternary Aden series are best developed in central Afar, where a distinction from the Afar series is somewhat arbitrary. Widely scattered Pliocene basalts on the rift margins and plateau interiors were erupted from small vents which occasionally produced basanites and melanephelinites (Le Basand & Mohr, 1968).

In the upper Pliocene, very voluminous fissural and central eruptions of trachyte-pantellerite ignimbrites covered most of the southern Ethiopian Plateau and filled the main Ethiopian rift (Mohr, 1968). The sources were situated chiefly at the rift margins where thicknesses of 300 to 500 m have been measured, but the thickness in the rift floor is probably much greater. Middle Pleistocene and later volcanism formed a chain of trachyte caldera volcanoes along the eastern rift from North Tanzania to Afar. Basalts are sometimes associated with these

centres, but more typical, particularly in the Aden series of Ethiopia, are silicic volcanics including ignimbrites/froth flows. The caldera volcanoes tend to be situated on the very young axial fracturing of the rift floor, and in the main Ethiopian rift and southern Afar are related to en echelon offsets of the Wonji fault belt (Mohr, 1967a, 1967c). In Ethiopia the younger basalts of the Aden Series were erupted in relatively minor volumes both on the rift floor and on the plateaus, including the Tana rift.

In the Salt plain of northern Afar, the multicentre Erta Ale basalt range has shown a variable but ever-present activity since its discovery (Tazieff and Varet, 1969). Basalt centres in both the Kenya and the Main Ethiopian rift have erupted within the last few hundred years, a period which probably also includes the youngest panttelarite obsidian lavas of some Ethiopian volcanoes (Mohr, 1962, 1966; Gibson, 1970).

2.5 VOLCANIC ASSOCIATIONS

Compared with East African volcanics, those of Ethiopia include a great abundance of Tertiary basalts and Plio-Pleistocene ignimbrites; among the latter, trachytic types are subordinate varieties having peralkaline rhyolite compositions. There is a notable absence of flood phonolites in Ethiopia, and nephenalinites are rather rare. The Afar series shows an association of alkali olivine basalt-mugerite-alkali trachyte. The Aden Series basalts are olivine-bearing alkaline types in

the main Ethiopian rift and southern Afar, and similar young lavas in the Tana rift are associated with basanites and phonolites (Comucci, 1950). The youngest basalts of northern Afar are distinctive, showing characters intermediate between those of the eastern rift and the Red Sea oceanic tholeiites (Barberi et al., 1970; Mohr, 1971b). They range from picritic basalts with tholeiitic chemistry and alkaline mineralogy to iron-rich andesine basalts (Tazieff and Varet, 1969) and are associated with minor quantities of iron-rich hayalo-trachaytes (extruded in a highly fluid state).

Voluminous Pliocene ignimbrites of south central Ethiopia have alkali trachyte-pantellerite compositions, and related lava centres include characteristic biotite-anorthoclase trachytes. Minor penecontemporaneous phonolites and nephelinites are probably not directly related to the ignimbrites. The Pliocene-Quaternary caldera volcanoes of the rift floor again show a trachyte-pantellerite association (Gibson, 1967), and the youngest Holocene lavas are typically pitchstones. Some of these silicic centres are marked by recent flank fissure eruptions of alkali olivine basalts, as well as open fissures not filled with lava. The grater abundance of basalts in Ethiopia can be related to the greater degree of crustal upwarping and dilatation (Wolde, 1989).

CHAPTER 3: THEORETICAL BACKGROUND

3.1 THE BASIC CONCEPTS OF GRAVITY

Every material body around us will begin to move towards the ground when it is released freely from a state of rest. This motion is caused by a force acting on the body and this force is called gravity.

The possible forces acting on a body of mass m (Fig. 4) on the surface of the Earth (Heiskanen and Moritz, 1967) are:

Assuming a spherical Earth, the attractive force of the Earth is given by

$$\mathbf{F} = - GMm\ \mathbf{R}/R^3 \qquad 1$$

where R is the radius of the Earth (6371 km), M its mass (6×10^{24}kg) and G the universal gravitational constant ($6.672 \times 10^{-11} m^3 s^{-2} kg^{-1}$).

The centrifugal force, due to the rotation of the earth about its axis of rotation is given by

$$\mathbf{f}_{cg} = - m\omega x(\omega \times \mathbf{R}) \qquad 2$$

and the z-component is

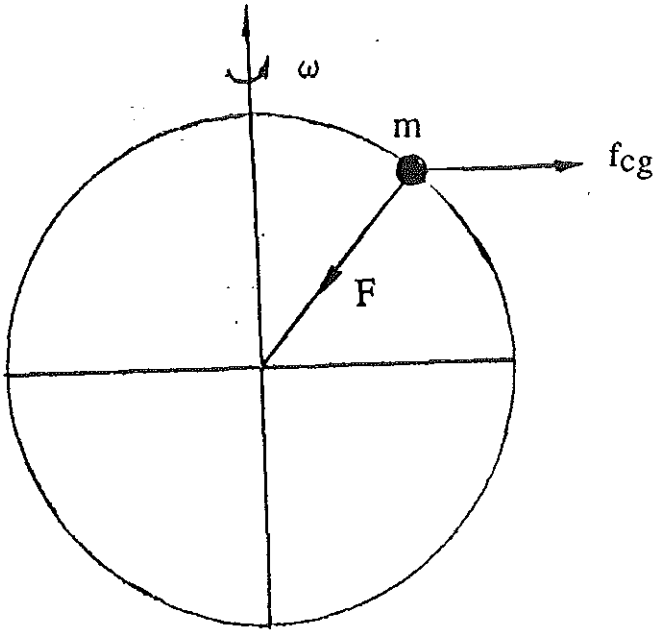

Fig.4 The components of the gravity force: attractive (F) and centrifugal (f_{cg}) forces, assuming spherical Earth.

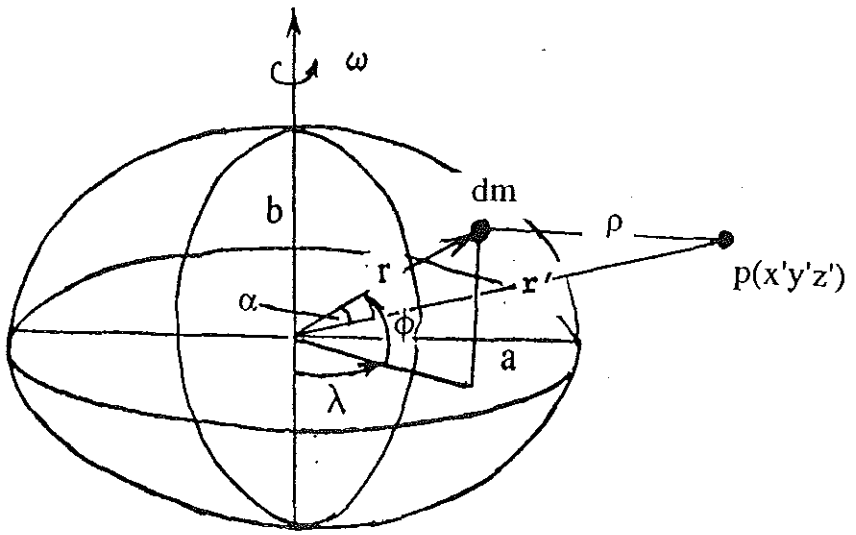

Fig.5 Figure of the Earth. a, equatorial radius of the earth; b, polar radius of the earth; ϕ the latitude angle; λ the longitude; ω the angular velocity of the earth.

$$(f_{cg})_z = -m\omega^2 R\cos\phi,$$

where ω is the angular velocity of the earth.

The coriolis force, if the body is moving on the surface of the Earth with velocity **V** given by

$$\mathbf{f}_{cor} = 2m\omega x\ \mathbf{V} \qquad 3$$

and the z-component is

$$(f_{cor})_z = 2mv\sin\phi$$

It is evident from Eq. 2 that the centrifugal force is maximum at the equator and zero at the poles and it opposes the attractive force of the Earth and from Eq. 3, the coriolis force is zero for a body at rest (V=0) on the surface of the Earth. By definition, the resultant of the attractive and centrifugal forces is the force of gravity. Hence the acceleration due to gravity (**g**) is given by

$$\mathbf{g} = -GM\ \mathbf{R}/R^3 - \omega\ x\ (\omega\ x\ \mathbf{R}) \qquad 4$$

To determine the gravity field of the Earth at a point we must know its shape and density distribution. Due to the centrifugal force, the Earth departs from a spherical shape; it is bulged at the equator and flattened at the poles. That is, the effect of the centrifugal force gives the earth the form of an

ellipsoid of revolution, a surface generated by the rotation of an ellipse about its minor axis with the major axis generating the equatorial plane.

Thus, for describing the earth's form, one usually used as a reference an ellipsoid of revolution with z-axis coinciding with the axis of the earth rotation and xy-plane with the equatorial plane (Sjöberg, 1990). The equation for such an ellipsoid reads:

$$(x^2 + y^2)/a^2 + z^2/b^2 = 1 \ , \qquad 5$$

where a is the semi-major axis and b is the semi-minor axis. The flattening (f), the first and second eccentricity (e,e') of the ellipsoid are defined as:

$$f = (a-b)/a, \quad e = (a^2 - b^2)^{1/2}/a \quad \text{and} \quad e' = (a^2 - b^2)^{1/2}/b$$

and these parameters are used to describe the deviation of an ellipsoid from a sphere, which has $f = e = e' = 0$.

The splitting of the gravity field into a "normal" and a remaining small "disturbing" field considerably simplifies the problem of its determination (Heiskanen and Moritz, 1967). Therefor we assume that the ideal reference ellipsoid, which is related to the mean sea level surface with excess land masses removed and ocean deeps filled, is an equipotential surface of a normal gravity vector field. Denoting the potential of the normal gravity field by

$$U = U(x, y, z), \qquad 6$$

we see that the reference ellipsoid is a surface with

$$U(x, y, z) = U_0 = \text{constant}. \qquad 7$$

The potential (U) of the normal gravity vector field is the sum of the attractive potential (V) and the centrifugal potential (Φ):

$$U = V + \Phi = G\int dm/\rho + \tfrac{1}{2}\omega^2(x^2 + y^2). \qquad 8$$

The normal gravity vector γ_ϕ at a given latitude ϕ on the reference ellipsoid is the gradient of U:

$$\gamma_\phi = -\,\text{grad}U \qquad 9$$

whose magnitude is the normal gravity and the direction is that of the plumb line, i.e., the plumb line is vertical at all points on the equipotential surface. For an external point P(x′, y′, z′) (Fig.5), who rotates with the earth at an angular velocity ω about the z-axis,

$$U = G\int dm/\rho + \tfrac{1}{2}(x'^2 + y'^2)\ \omega^2 \qquad 10$$

and

$$1/\rho = 1/r'[1 - 2r/r'\cos\alpha + r^2/r'^2]^{-\frac{1}{2}}. \qquad 11$$

Provided $|2(r/r')\cos\alpha - r^2/r'^2|<1$, the bracketed quantity may be expanded by the binomial theorem to give

$$1/\rho = (1/r')[P_0(\cos\alpha) + (r/r')P_1(\cos\alpha) + (r/r')^2\ P_2(\cos\alpha)+...] \qquad 12$$

and

$$U = G/r'\left(\int dm + (1/r') \int P_1(\cos\alpha)\ r\ dm + (1/r'^2) \int P_2(\cos\alpha)\ r^2\ dm \right.$$
$$\left. +\ldots \right] + \tfrac{1}{2}(x'^2 + y'^2)\ \omega^2\ , \qquad 13$$

where the functions $P_n(\cos\alpha)$ are Legendre polynomials. Using the definition of moment of inertia in mechanics one can arrive at

$$U = MG/r\ [1 + (K/2r^2)(1 - 3\sin^2\phi) + \omega^2\ (r^2/2MG)\ \cos^2\phi], \qquad 14$$

where M is the total mass of the earth, and K is a constant determined by the moments of inertia about x, y, and z axes and the mass M (Gerland, 1979, Tsuboi, 1983; Telford et al., 1990, Heiskanen and Moritz, 1967). Hence, using Eqs.9 & 14, one can easily show that the normal gravity (theoretical gravity) value, γ_ϕ, as a function of the latitude angle, ϕ, at any point on this ellipsoid is given by

$$\gamma_\phi = \gamma_0\ (1 + B_1\ \sin^2\phi - B_2\ \sin^2 2\phi) \qquad 15$$

where γ_0 is the value of γ_ϕ at the equator ($\phi = 0$), B_1 and B_2 are constants. Making use of all the observed values of g at a number of points over the earth, numerical values of the constants B_1 and B_2 have been determined in 1930 by the International Association of Geodesy (IAG) and adopted the formula known as **the 1930 International Gravity Formula** and is given by

$$\gamma_{\phi 1930} = 978049(1+0.0052884\sin^2\phi - 0.0000059\sin^2 2\phi)\ \text{mGal} \qquad 16$$

with γ_0 = 938049 mGal, equatorial radius a= 6378.388 km, polar radius b=6356.909 km, the elipticity (polar flattening) given by f=(a-b)/b=1/297.

Recent studies on the orbits of satellites have provided more precise values for constants B_1 and B_2 and the following is the revised theoretical gravity formula established by IAG in 1967

$$\gamma_{\phi 1967} = 978031.85(1+0.0053024\sin^2\phi-0.0000059\sin^2 2\phi) \text{ mGal} \quad 17$$

With γ_0 = 978031.85 mGal, a = 6378.160 km, b = 6356.909 km, and f=1/298.25.

Even in its most refined state, the standard theoretical gravity formula (Eq. 17) is a very crude approximation. It assumes that there are no undulations on the Earths' surface, where as, in fact, we have elevated lands (hills) and oceanic depressions. Hence, for a practical work,i.e., measurement of gravity on the physical surface of the Earth we must define a physical equipotential surface on the Earth. This physical surface is known as the **Geoid.**

Geoid is a surface such that gravity **g** is perpendicular to it.

Geoid is a zero reference (elevation datum h = 0) for elevations and ocean depths, as given on topographic maps.

Geoid is the undisturbed mean sea level surface continued into

continents so as to encircle the Earth, water seeking its level in imaginary shallow canals until it is at rest.

The value of gravity at a point calculated by the standard theoretical formula (Eq. 17) and that observed and reduced to the geoid do not agree with each other. This is because the effect of attraction of an invisible anomalous mass under the point is involved in the observed value. The small difference between the actual gravity potential W and the normal (theoretical) gravity potential U is denoted by T (Fig. 6) (Heiskanen and Moritz, 1967) so that

$$W(x, y, z) = U(x, y, z) + T(x,y,z) \qquad 18$$

T is called the anomalous potential, or disturbing potential.

We compare the potential on the geoid

$$W(x, y, z) = W_0$$

with the potential on the reference ellipsoid

$$U(x, y, z) = U_0$$

of the same potential $U_0 = W_0$. Consider now the gravity vector g_P at a point P of the geoid (Fig.6) and the normal gravity vector γ_Q at a point Q of the ellipsoid. The **gravity anomaly vector Δg** is defined as their difference:

$$\Delta g = g_P - \gamma_Q \qquad 19$$

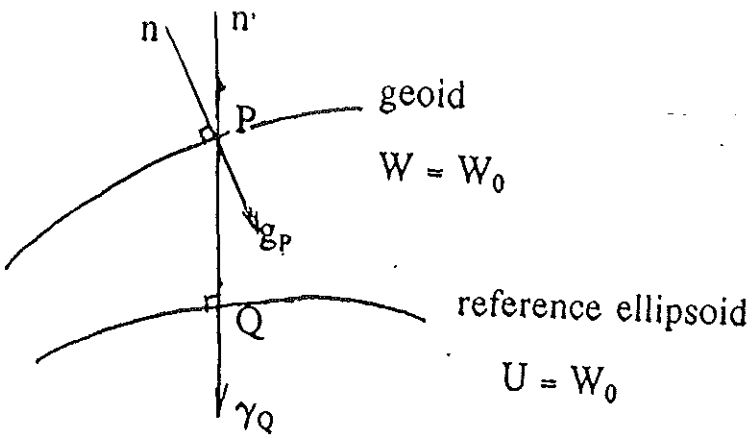

Fig.6: Geoid and Reference Ellipsoid. n and n' are the unit normals to the geoid and ellipsoid respectively.

A vector is characterised by magnitude and direction. The difference in magnitude is the gravity anomaly given by

$$\Delta g = g_P - \gamma_Q \qquad 20$$

the difference in direction is the deflection of the vertical (θ). Here, g_P is the gravity value observed (g_{obs}) at a point on the surface of the Earth and reduced to the geoid point (P). γ_Q is the theoretical gravity value on the ellipsoid point (Q).

Gravity anomalies develop in consequence of differences in the density distribution of the earth, particularly in the upper layers known as the crust. Therefore, they reflect the internal constitution of the crust and indicate the presence of various geological structures connected with the dislocation of rocks of different densities. This enables us to study the internal structure of the earth and for gravity prospecting.

3.2 GRAVITY REDUCTIONS

As noted above, if g_{obs} is the observed value of gravity on the land surface at a height h above the geoid, it must be reduced to the latter through the application of different reductions before it is compared to γ_ϕ. The reductions must attempt to produce the value of gravity that would have occurred if it were possible to observe on the geoid. The operation is known as gravity reduction.

There are many such reductions; however, only the major concepts are discussed: free air, Bouguer, terrain, isostatic, and latitude correction.

3.2.1 FREE AIR REDUCTION

Since gravity varies inversely with the square of distance, it is necessary to correct for changes in elevation between stations to reduce gravity readings to a datum plane (geoid). This is called free air correction. The free air correction does not take account of the material between the station and the geoid. If the elevation of a gravimeter is changed, its distance from the centre of the Earth changes by the same amount. From the inverse-square law, considering the Earth as a globe, the value of gravity at sea level (geoid) is (dropping the minus sign) obtained from Eq. 1.

$$g = GM/R^2$$

The gravity at a point located at a height h above the geoid is

$$g_h = GM/(R+h)^2.$$

By the Binomial expansion

$$g_h = GM/R^2\ (1 - 2h/R + 3h^2/R^2 - \ldots)$$
$$= g - 2gh/R + \ldots.$$

From this expression, the free air correction (δg_{FA}) is written as

$$\delta g_{FA} = g - g_h = 2g_m/R_m \qquad 21$$

where R_m and g_m are the average radius and gravity of the Earth, respectively. Thus, with the average values R_m = 6371 x 10^3 m and g_m = 980 Gal inserted, the free air correction for h measured in meters is δg_{FA} = 0.3086h Mgal. The free air correction is added to gravity reading when the station is above the geoid and subtracted when below it.If this correction is applied to the observed gravity g_{obs} then the anomaly obtained by subtracting the standard theoretical gravity value at the given latitude is called free air anomaly (Δg_{FA}). Therefore, it is given by

$$\Delta g_{FA} = g_{obs} + \delta g_{FA} - \gamma_\phi$$
$$= g_{obs} + 0.3086\ h - \gamma_\phi \qquad 22$$

3.2.2 BOUGUER REDUCTION

The attraction of the slab of density ρ that exists between the gravity station and the geoid, which was ignored in the free air correction, is obtained by calculating the effect of an infinite disc. It is given by

$$\delta g_B = 2\Pi G\rho h \qquad 23$$

where h is the height of the gravity station above the geoid and G is the universal gravitational constant. For mean crustal density (2.67 g\cm^3) and h in meters, the Bouguer correction reduces to

$$\delta g_B = 0.1119h.$$

This is referred to as the Bouguer reduction, which moves the mass between the Earth's surface and the geoid to infinity and then reduces the point to the geoid. The Bouguer correction is applied in opposite sense to the free air correction, i.e., it is subtracted when the station is above the geoid and vice versa.

3.2.3 TERRAIN CORRECTION

Nearby hills above the elevation of the gravity station exert an upward pull on the gravimeter, whereas valleys (lack of material) below it fail to pull downward on it. Thus, both the

hills and valleys always reduce the observed gravity value and the terrain correction is always added to the station reading. The usual procedure in making corrections for such distortions is to calculate the attraction of all the mass that would have to be added to the valleys below and all that would have to be removed from the hills above to give perfectly flat topography having the same elevation as the station. Calculation of the attraction of irregular topographic elements is greatly facilitated by the use of special templates and tables, such as the Hammer chart, designed for the purpose. The chart, printed on transparent sheeting, is superimposed on a topographic map of the area around the gravity station and has the same scale as the chart. It consists of a series of concentric circles, whose centre is placed over the gravity station on the map, with radial lines dividing the zones between the circles into compartments. The gravity effect of a single sector is given by

$$\delta g_{sec}(r,\theta)=G\rho\theta\{(r_0-r_i)+(r_i^2+h^2)^{1/2}-(r_0^2+h^2)^{1/2}\} \qquad 24$$

where G is the universal gravitational constant, θ is sector angle in radians, $h = /e_s - e_a /$, e_s is the station elevation, e_a is the average elevation in the sector, and r_0 and r_i are the outer and inner sector radii. The terrain correction δg_T is the sum of the contribution of all the sectors:

$$\delta g_T(r,\theta) = \Sigma_r \Sigma_\theta \delta g_{sec}(r,\theta) \qquad 25$$

When this correction, together with the free air, and Bouguer

reductions, is applied to the observed gravity, the resulting anomaly obtained by subtracting the standard theoretical gravity value at the given latitude is called **Bouguer anomaly** (Δg_B) and is given by

$$\Delta g_B = g_{obs} + 0.3086h - 0.1119h + \delta g_T - \gamma_\phi \qquad 26$$

3.2.4 ISOSTATIC REDUCTION

The standard theoretical formula makes no allowance for the lateral density variations in the Earth. It is assumed that the density is the same every where at the same distance below the surface. Yet where isostatic compensation exists there must be lateral changes in the subsurface density, causing this assumption to be violated. To reduce the discrepancy, an isostatic correction is made on the basis of surface elevation data, the form of the correction depending on the isostatic model, e.g., Pratt or Airy, assumed. Once the data have been corrected for predicted isostatic effects (along with the terrain, free-air and Bouguer corrections) the residual between the observation so corrected and the predicted value at the latitude of the station is referred to as the **isostatic anomaly.** If perfect isostatic compensation exists, this anomaly is zero. If the anomaly is positive over land, there is a deficit of compensation. If it is negative, the area is considered to be overcompensated.

3.2.5 LATITUDE CORRECTION

The centrifugal force due to the rotation of the Earth, which opposes the attractive force, is maximum at the equator and zero at the poles. The polar flattening increases the attractive force at the poles by making the geoid closer to the Earths' centre of mass. Thus, both the rotation of the Earth and its equatorial bulge produce an increase of gravity with latitude. To reduce this effect we use the latitude correction (δg_L). It is obtained by differentiating the standard theoretical gravity formula (Eq.15) with respect to the north-south horizontal distance ($\Delta s = R_e\, \delta\phi$) or the latitude angle ϕ, i.e.,

$$\delta g_L/\delta s = (1/R_e)\ \delta g_\phi/\delta\phi = 0.811\ \sin 2\phi\ \text{mGal/km} \qquad 27$$

where R_e is the radius of the Earth (= 6371 km).

At 45^0 latitude, the variation is about 0.01 mGal for each 13 m of north-south displacement and it is zero at the equator and poles. It indicates that positions must be known to better than 30.5 m in the north-south direction where an ultimate precision of 0.02 mGal is desired. The correction is added to the observed gravity g_{obs} as we move toward the equator.

3.3 GRAVITY CORRECTIONS

Gravity corrections are of many kinds, but they can be classified as follows:

1. Instrumental correction,
2. Earth-tide correction.

3.3.1 INSTRUMENTAL CORRECTION

All gravimeters change null reading with time, even when set up at a fixed station. This continual variation of the gravity readings with time is known as **drift**. This drift is the result mainly of creep in the springs. In addition, if the movement is not clamped between readings, or is subjected to sudden motion or jarrging during transport, the change may be somewhat erratic. The net result of drift is that, over a period of days or even hours, repeated readings at one station will give a series of different gravity values.

Some of the stations were occupied periodically during the field work in order to produce a drift curve for the LaCost & Romberg gravimeter. The difference between two readings at a station were plotted against the time and a straight line drift curve was drawn. The intermediate gravity stations, occupied only once,were corrected for the drift which has occurred during the appropriate fraction of time interval between repeat readings at the station, keeping in mind that positive drift

requires negative correction and vice-versa.

3.3.2 EARTH-TIDE CORRECTION

Gravimeters are sensitive enough to respond to the gravitational attraction of the Sun and Moon and register the periodic changes in the attraction caused by the movements of the Earth with respect to these bodies. These changes of gravity are known lunar and solar variations. The magnitude of these changes varies with latitude, time of month, and time of year, but the complete tidal cycle is accompanied by a gravity change of only 0.2 to 0.3 mGal. The corrections can be calculated from the knowledge of the locations of the Sun and Moon. For this purpose special tables exist giving the value of the lunar and solar variation for every latitude and longitude at any hour of the day or night and every day of the year. However, because the variation is smooth and relatively slow, usually it is included in the instrumental drift correction.

CHAPTER 4: THE BOUGUER GRAVITY ANOMALY

4.1 THE GRAVITY DATA

The simple Bouguer anomaly map presented in Figure 7 was compiled from approximately 862 gravity observations represented by dots on the Bouguer anomaly map. The data sources include gravity data collected by the author and his supervisor Dr. Abera Alemu during January 1993 and March 1993 using the LaCoste and Romberg, Model G # 781 gravimeter of the Geophysical Observatory, Leeds University, data from Ebinger, (1990), Marsden, (unpublished data), the Ethiopian Geological Survey, Kenyan gravity catalog (Swain and Khan, 1977), and Alemu (1992). The station spacing is quite variable, but the average spacing is between 5 and 10 km.

The above data sets were merged and referred to the IGSN71 (Morelli et al., 1971) gravity datum. The primary gravity base of the Geophysical Observatory (977452.16 mGal) of Addis Ababa University, which is referred to the IGSN71 Datum by the US DMA Aerospace Centre, was used. The normal gravity, γ_ϕ, at latitude ϕ of each station, has been calculated from the 1967 gravity formula (Moritz, 1971).

The approximation :

$\gamma_\phi = 978031.85(1 + 0.0053024 \sin^2\phi + 0.0000059 \sin^2 2\phi)$ mGal,

which is accurate to ± 0.4 mGal, has been used.

4.2 ELEVATION AND COORDINATES OF THE GRAVITY STATIONS

For stations occupied in the study area elevations were determined using altimeters; Trigonometric points, bench marks, and spot heights established by the Ethiopian Mapping Authority (EMA) in the study area were used as base stations for elevation control.

Two Paulin System surveying altimeters were used. The scales of these instruments have been calibrated on control points with an altitude difference of about 2000m. An accuracy of ±10m for the altimetric observations giving an error in the Bouguer anomaly of ± 1.967 mGal may be guaranteed.

A uniform determination of the geographic coordinates was not possible everywhere, because a unique set of maps did not exist, for example of scale 1: 50,000, covering the entire area. At worst, we had to use maps of a scale 1: 250,000. In such cases, the positioning error amounts to about 300 m, which corresponds to about ± 0.06 mGal, caused by the effect of imprecise latitude.

Free air and Bouguer corrections were made using sea level as the datum and 2.67 g/cm^3 as the reduction density. Terrain correction was not applied but was treated as a systematic error ($s_{\Delta g}$) assuming that its effect is not greater than ± 2 mGal (Alemu, 1992). The overall accuracy of the Bouguer anomaly values at each station is estimated at ± 2.842 mGal.

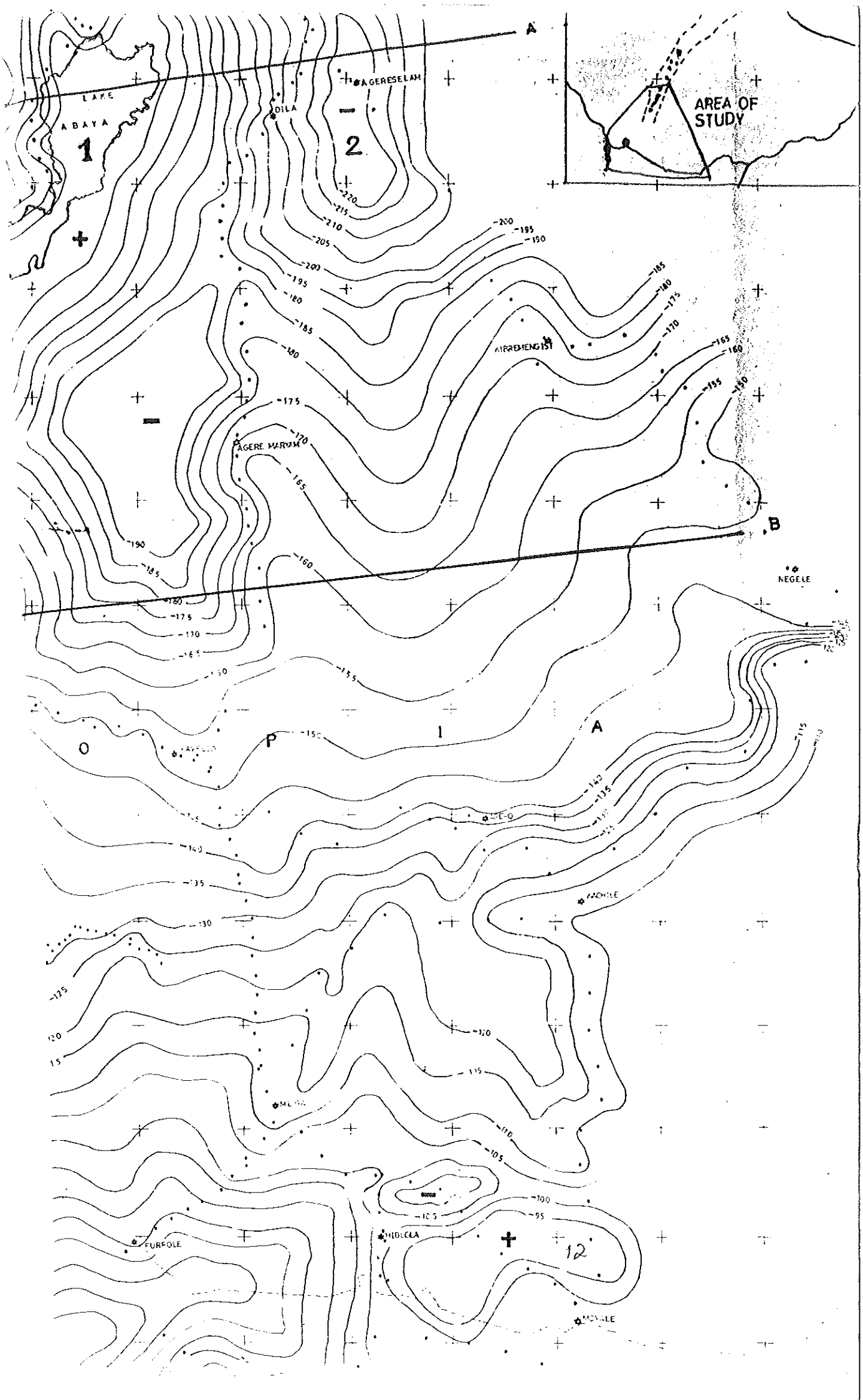
A
B
LAKE
ABAYA
1
2
DILA
AGERESELAH
AREA OF STUDY
AIRREMENGIST
AGERE MARIAM
NEGELE
ACHILE
FURFOLE
HIDLELA
MOYALE
12

After editing the resulting data file was plotted on a 1:250,000 scale map and contoured at 5 mGal interval (Fig. 7). The contouring was done by hand.

4.3 ASSESSMENT OF ERRORS IN THE GRAVITY ANOMALIES

The overall mean square error $\varepsilon^2_{\Delta g}$ of the gravity anomalies Δg is computed according to:

$$\varepsilon^2_{\Delta g} = \sigma^2_{\Delta g} + s^2_{\Delta g} \qquad 28$$

where $\sigma_{\Delta g}$ is the standard error (due to random errors) and $s_{\Delta g}$ is the systematic error (bias) (Sjöberg, 1990) introduced in the computation of Bouguer anomalies by neglecting the correction for irregularities in the terrain (terrain effect).

The variance $\sigma^2_{\Delta g}$, is computed according to the law of propagation of errors as:

$$\sigma^2_{\Delta g} = \sigma^2_g + (\partial \Delta g/\partial \phi)^2 \sigma^2_\phi + (\partial \Delta g/\partial h)^2 \sigma^2_h \qquad 29$$

where σ_g, σ_ϕ and σ_h are the standard errors in determining the gravity (observation error), the latitude and elevation of the gravity points respectively.

The standard error σ_g, is obtained by computing the internal variance (Bjerhammer, 1973) of 30 independent observations (Table 1) made on 10 gravity check points, that means, 3

independent observations on each check point using the formula:

$$\sigma^2_g = (\Sigma_{s1}(vv) + \Sigma_{s2}(vv) + \ldots + \Sigma_{s10}(vv)\}/(n-s) \qquad 30$$

where n is the total number of independent observations, s1,s2...,s10 are the number of gravity check points, and v are residuals for the individual observations at each check point. The computed standard error σ_g (observation error) amounts to ±0.42 mGal.

Table 1. Table of observed gravity values (mGal) for computing the internal variance (for 10 check points)

y	$\hat{y}$	V	VV	
7520.56	7520.47	0.09	0.0081	
7520.46	7520.47	-0.01	0.0001	
7520.40	7520.47	-0.07	0.0049	$\hat{y}_1 = 7520.47$
7516.76	7516.06	0.70	0.4900	
7515.91	7516.06	-0.15	0.0225	
7515.51	7516.06	-0.55	0.3025	$\hat{y}_2 = 7516.06$
7674.37	7674.47	-0.10	0.0100	
7674.84	7674.47	0.37	0.1369	
7674.19	7674.47	-0.28	0.0784	$\hat{y}_3 = 7674.47$
7635.67	7635.53	0.14	0.0196	
7635.87	7635.53	0.34	0.1156	
7635.06	7635.53	-0.47	0.2209	$\hat{y}_4 = 7635.53$
7613.94	7614.00	-0.06	0.0036	
7613.91	7614.00	-0.09	0.0081	
7614.15	7614.00	0.15	0.0225	$\hat{y}_5 = 7614.00$
7731.13	7731.22	-0.09	0.0081	
7731.19	7731.22	-0.03	0.0009	
7731.35	7731.22	0.13	0.0169	$\hat{y}_6 = 7731.22$
7727.23	7727.19	0.04	0.0016	
7727.29	7727.19	0.10	0.0100	
7727.04	7727.19	-0.15	0.0225	$\hat{y}_7 = 7727.19$
7811.39	7811.22	0.17	0.0289	
7811.43	7811.22	0.21	0.0441	
7810.85	7811.22	-0.37	0.1369	$\hat{y}_8 = 7811.22$
7835.94	7835.35	0.59	0.3481	
7834.41	7835.35	-0.94	0.8836	
7836.09	7835.35	0.74	0.5476	$\hat{y}_9 = 7835.35$
7609.24	7609.36	-0.12	0.0144	
7609.40	7609.36	0.04	0.0016	
7609.45	7609.36	0.09	0.0081	$\hat{y}_{10} = 7609.36$

For the positional error $R\sigma_{\varphi}$ = ± 300m previously adopted in fixing the latitude φ of a station from the 1:250,000 topomap of the region, the corresponding error estimate in the normal gravity is computed by Eq.27:

$$\varepsilon_{\phi} = 1/R(\partial\gamma/\partial\phi)R\sigma_{\phi}=(0.812 \sin 2\phi)\sigma_{\phi} \text{ mGal/km}$$

where R is the mean radius of the earth. The computed error estimate amounts to ± 0.06 mGal for $\phi = 7^0$ (i.e for the mean latitude of the study area).

By differentiating the expression for the Bouguer anomaly formula (Eq.26) with respect to station height h, the rate of change of the combined free-air and Bouguer correction with elevation at a station may be expressed by

$$\partial\Delta g/\partial h \approx 0.3086 - 0.0419\rho \qquad 31$$

or with the standard density 2.67g/cm^3

$$\partial\Delta g/\partial h \approx 0.1967 \text{ mGal/m} \qquad 32$$

The maximum error estimate in the Bouguer anomaly corresponding to the previously adopted maximum elevation error, σ_h = ± 10m of a gravity station is computed by the relation, $\varepsilon_h = (\partial\Delta g/\partial h)\sigma_h$ and amounts to ± 1.967 mGal.

The combined root mean square error $\varepsilon_{\Delta g}$, of the gravity

anomalies Δg is therefore estimated according to the relation

$$\varepsilon_{\Delta g} = (\sigma^2_g + (\partial \Delta g/\partial \phi)^2 \sigma^2_\phi + (\partial \Delta g/\partial h)^2 \sigma^2_h + s^2_{\Delta g})^{1/2} \quad 33$$

and amounts to ± 2.84 mGal. The overall accuracy of the Bouguer anomaly values (assuming the correct density has been chosen) is therefore expected to be around ± 2.84 mGal. Figure 7 shows the derived Bouguer anomaly map of the study area contoured at 5 mGal intervals. As the magnitude of a contour interval used to produce gravity anomaly maps depends on the uncertainty of the gravity anomalies, the contour interval chosen here can be reasonably accepted.

4.4 OVERVIEW OF THE BOUGUER GRAVITY ANOMALY MAP

There are Bouguer gravity anomalies associated with specific geologic features (e.g., high-grade metamorphic complexes, Tertiary volcanics, and Quaternary sedimentary basins). The anomalies have a total relief of 175 mGal, ranging from -45 mGal at Turkana in northern Kenya to -220 mGal at Agere Selam, about 50 km northeast of the Abaya-Chamo rift. The latter is the lowest Bouguer anomaly recorded over the study area. The anomaly contours north of latitude (ϕ=4^{0}30′) have a typical N-S to NNE-SSW trend and those south of latitude (ϕ=4^{0}30′) an E-W to NNW-SSE trend which is similar to the structural trend of the individual rift segments and the associated rift shoulders. The contour map displays complex patterns with alignment of positive and negative anomalies of varying dimensions. To

discuss all the individual anomalies is beyond the scope of this thesis. Hence, the analysis of the Bouguer gravity anomalies (Fig. 7) associated with the Abaya-Chamo rift, the Chew Bahir rift, and some prominent gravity anomalies in the surrounding areas will be given to illustrate the general trends. The anomalies discussed below are numbered on Figure 7.

A positive Bouguer anomaly (anomaly 1) of -165 mGal occurs over the floor of the Abaya-Chamo rift and is flanked by negative anomalies (anomalies 2 and 3) on the shoulders. This is a superposition of a narrow positive anomaly on a larger negative one. The gravity survey described for the northern extension of the MER (Alemu, 1992; Alemu and Sjöberg, 1990), the Afar depression (Makris et al.,1972), the Gregory rift (Searle, 1970) has shown this pattern is a typical characteristics of the gravity field of the East African rift system. In general, the axis of the positive anomaly corresponds to the rift axis. However, there are local variations in the trend of the positive anomaly, which is offset in places. To the north of Lake Abaya, a gravity minimum (anomaly 4) of -200 mGal occurs over ignimbrites and pumices of the rift floor and Lacustrine deposits.

Southwest of the southern end of the Abaya-Chamo rift which is the southern termination of the MER lies the Chew Bahir rift. The anomaly pattern observed here is completely different from that of the Abaya-Chamo rift. Unlike the MER and the Gregory rift, a negative anomaly (anomaly 5) of magnitude -135 mGal

occurs over the Chew Bahir rift floor and is flanked by positive anomalies (anomalies 6 and 7) on the shoulders. The positive anomaly (anomaly 6) on the eastern shoulder with magnitude -100 mGal is associated with Boran and Konso uplifts (Fig. 2 and 3) which according to the geologic map of Merla et al., (1973) are composed of various types of schists and amphibolites, and Tertiary basalts. The negative anomaly (anomaly 5) along the rift axis occurs over Pleistocene lacustrine and swamp deposits of the rift floor. The positive anomaly (anomaly 7) on the western shoulder of the rift, with magnitude -75 mGal is associated with the Hamer horst which is composed of various types of schists and amphibolites. West-southwest of the Hamer horst, the gravity field decreases towards the Pleistocene to recent beds Lacustrine, swamp, and alluvial deposits of the Lake Turkana-Lower Omo river depression.

South of the Chew Bahir rift in northern Kenya, the trend of the gravity anomalies strikes SE-NW and SSE-NNW with alternating bands of positive and negative anomalies. This trend of the gravity anomalies is consistent with the trend of the geological features there.

The positive anomaly (anomaly 8), with magnitude -65 mGal and trending in a NW-SE direction occurs over a block of Pleistocene fissural basalts. The negative anomaly (anomaly 9), with magnitude -80 mGal trending in a SSE-NNW direction occurs at about $\phi = 3^0 35'$ and $\lambda = 36^0 25'$ over a block of Oligocene to

Pliocene fissural basalts. The positive anomaly (anomaly 10), with magnitude -45 mGal trending in a SSE-NNW direction occurs at about $\phi = 3^0 15'$ and $\lambda = 36^0 50'$ over the zone of Kinu Sogo fault belt (Fig. 1 & 7) which forms the northward continuation of the Kenyan (Gregory) rift. This is a zone of Pleistocene faults of small throw crossing the crest of a very shallow rise composed of Oligocene to Miocene fissural basalts. The negative anomaly (anomaly 11), with magnitude -105 mGal trending in an E-W direction occurs at about $\phi = 3^0 25'$N and $\lambda = 37^0 40'$E over the Huri hills which are composed of Quaternary fissural basalts.

The positive anomaly (anomaly 12) north of Moyale, with magnitude -95 mGal trending in an E-W direction occurs over a block composed of various types of schists and amphibolites.

CHAPTER 5: CRUSTAL MODELS

5.1 MODELLING AND DISCUSSION

The above overview of the Bouguer gravity field of the surveyed region indicates the complexity of the area. To obtain a better understanding of the sources of the gravity field, gravity models were constructed trending from Western Plateau through the rift to the Eastern Plateau. These models are an attempt to explain the crustal structure of the area and not necessarily to explain the near surface geology.

The profiles are marked AA and BB on the Bouguer anomaly map (Fig. 7) and their locations are chosen to illustrate the general crustal structure of the region. Values of the Bouguer anomalies extracted from the contours of Figure 7 at a 5 km spacing, and the corresponding elevation profiles are shown in Figs. 10-11. The profiles run through the major tectonic units (the plateaus and the rift) of the region. These units are comprised of tectonic dislocations (regions of crustal attenuation) along the axis of the rift and the bounding plateaus. For profile AA gravity maxima and minima define the structures associated with the rift floor and the plateaus respectively. However, what "happened" to profile BB is just the opposite of profile AA, i.e., the Chew Bahir Rift shows negative anomaly whereas the bounding high lands are associated with positive anomaly. A glance at profile AA shows, that the gravity anomalies have a sinusoidal nature, alternatively

positive and negative.

The gravity model used for the interpretation is shown in Fig.8. The model was constructed using a 2½-D gravity forward modelling algorithm of Rasmussen and Pederson (1979) given below.

$$\Delta g_z(r_0) = -2Y\, G_\rho \sum_i \mathbf{z}\cdot\mathbf{n}_i \log[(u_{i+1} + R_{i+1})/(u_i+R_i)] + 2G_\rho \sum_i \Big[(x_i z_{i+1} - z_i x_{i+1})/(\Delta x_i^2 + \Delta z_i^2) \Big\{ \Delta z_i \log[r_{i+1}(R_i + Y)/r_i(R_{i+1} + Y)] + \Delta x_i \left(\tan^{-1}(u_{i+1}Y/w_i R_{i+1}) - \tan^{-1}(u_i Y/w_i R_i)\right)\Big\}\Big], \qquad 34$$

where (U,V,W) is a coordinate system obtianed by rotating the (X,Y,Z) coordinate system so that V = Y, U = $(X_{i+1}, 0, Z_{i+1})$ and W = U X V and **n** is the outward directed normal to the surfaces in the X-Z plane; $U_i = X_i \cos\varphi_i + Z_i \sin\varphi_i$; $U_{i+1} = X_{i+1} \cos\varphi_i + Z_{i+1} \sin\varphi_i$ and $W_i = W_{i+1} = -X_i \sin\varphi_i + Z_i \cos\varphi_i$.

A full account of on the above formula is given in Rasmussen and Pederson (1979). This algorithm employs the well known 2-D formulae of Talwani (1973) and Talwani et al. (1959) but slightly changed to represent a 2½-D body, i.e a body of polygonal cross section with the tails in the strike direction cut off.

The profiles trend perpendicularly to most of the anomalies (e.g., the positive gravity maxima associated with the rift axis). Since there exists an established similarity between the

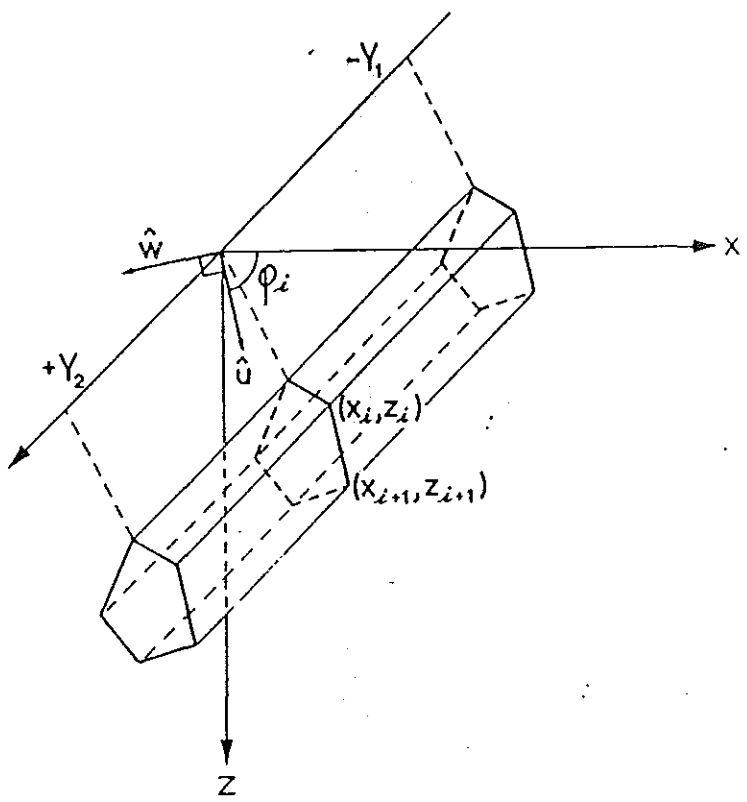

Fig.8 2½-D body. Strike direction is the y-direction. The 2½-D body is asymmetrical for Y_1 and Y_2 and symmetrical for $Y_1 = Y_2$. The end faces have their normals in the y-direction, and the other faces have their normals in the x-z plane (after Rasmussen and Pederson, 1979).

crustal structures of the MER and the Kenyan rift, results of the Kenyan Rift International Seismic project (KRISP) data of Griffiths et al., (1972), Khan et al., (1987) and Keller et al., (1992) performed in the northern and central parts of the Kenyan rift were used to constrain the crustal density models. As a starting point in the modelling the densities for the basalt and sedimentary cover (2.5 g/cm^3), upper crust (2.75 g/cm^3), lower crust (2.80 g/cm^3), anomalous mantle (3.00 g/cm^3), and the normal mantle (3.35 g/cm^3) were inferred from velocities determined from the seismic profiles.

The velocities of individual layers were converted to densities using the Nafe and Drake (1963) curves for the shallow rocks and the Birch (1961) and Henkel et al. (1990) relationship for the deeper crustal and upper mantle rocks (Fig. 9).

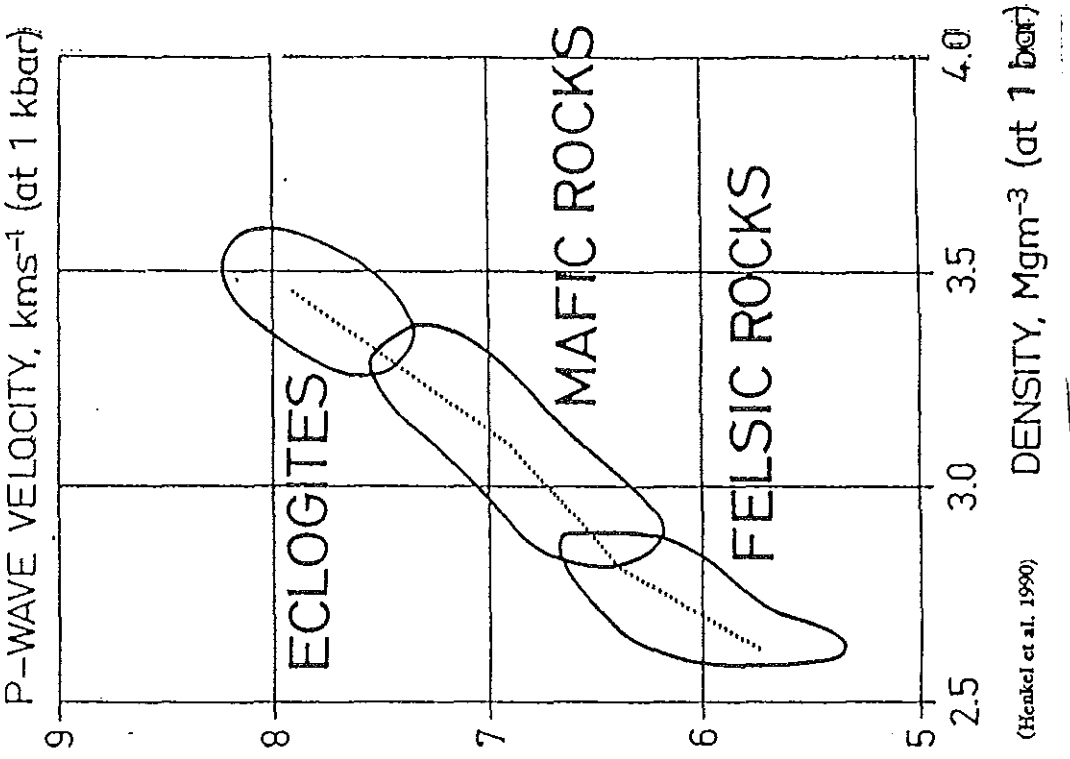

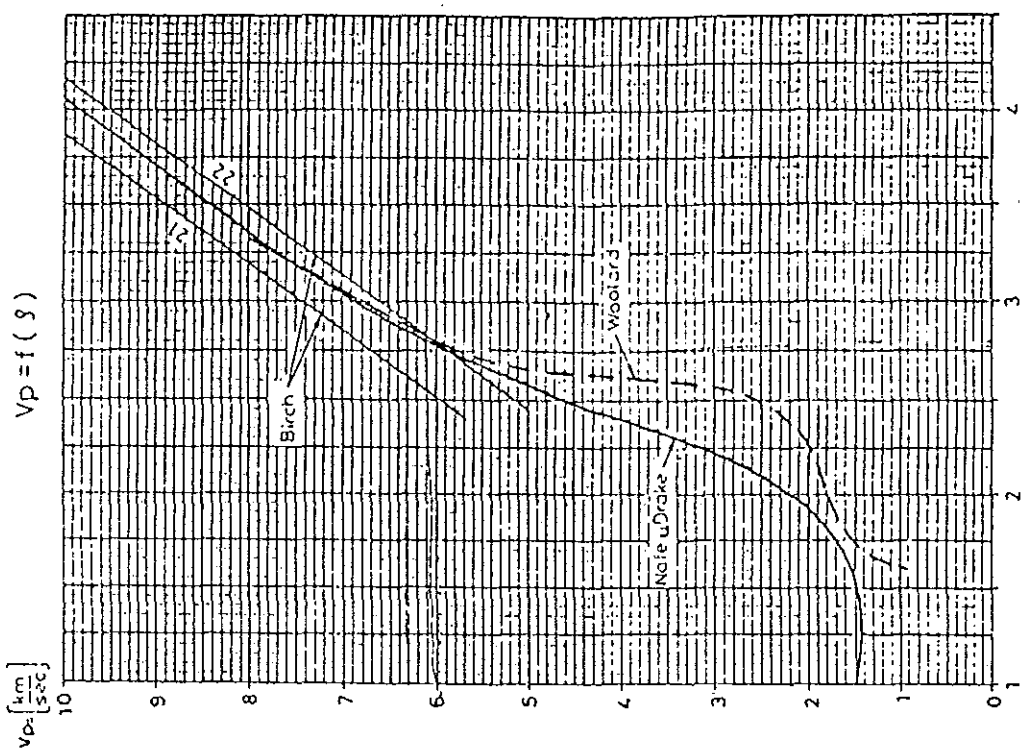

Fig. 9 : P-wave velocity-density curves used to convert the seismic velocities to density models. The curves have been taken from Nafe and Drake, 1974, Birch, 1961, Woolard, 1959 and Henkel et al., 1990.

The following table summarizes the estimated densities for the computation of the 2-dimensional gravity models. The lower limit of the anomalous mantle density is used in the model calculations.

Table 2. Estimated densities of crustal and upper mantle layers in the Main Ethiopian Rift based on Fig.9

Density interval (g/cm^3)	Velocity interval (km/s)	Layer Type
2.40-2.45	3.40-4.50	sedimentary basin
2.70-2.78	6.00-6.40	upper crust
2.80-2.95	6.60-7.20	lower crust
3.00-3.20	7.30-7.60	anomalous mantle
3.35	8.00	normal mantle

Since the gravity model is a function of densities (ρ) and depths (z) of the different crustal layers, the densities are fixed prior to modelling while depths are varied. The computations are carried out by comparing the calculated gravity effect of the polygonal layers with the observed

gravity at several points along a profile until the best fit was obtained. The observed gravity values taken from the contour map of Figure.7 along each of the two profiles are used in the computations.

5.2 2½-D CRUSTAL MODELS ALONG THE SELECTED PROFILES

The two gravity profiles shown on the Bouguer gravity map (Fig.7) are drawn along an E-W direction. Profile AA crosses the southern end of the MER and profile BB the Chew Bahir rift. The crustal density model with observed and calculated Bouguer gravity values and the corresponding elevation values is done for both profiles AA and BB.

The density models computed along these profiles are constructed in such a way that they consist of three crustal layers (sedimentary basin with ρ = 2.50 g/cm^3, upper crust (crystalline basement) with ρ = 2.75 g/cm^3, lower crust with ρ = 2.8 g/cm^3) layers , an anomalous mantle layer with ρ = 3.00 g/cm^3 and a normal mantle with ρ = 3.35 g/cm^3). An initial crustal thickness of 40 km, whose value is derived from the seismic refraction results of Makris and Ginzburg (1987) and results of crustal investigations by Herbert and Langston (1985) using teleseisms on the Western Plateau was used.

5.2.1 Profile AA (Chencha - Arbaminch- Hagereselam)

This profile (Fig.10) is 220 km long and starts from the

Western Plateau and crosses the Abaya-Chamo rift and the Amaro horst. The profile thus crosses the three major tectonic units (the plateaus and the rift) in a NNW-SSE direction in this region.

The western end of the profile starts with a negative gravity anomaly of -155 mGal (Fig.7), to the east it crosses the 20 km wide negative gravity anomaly of -185 mGal over the Chencha horst, the 30 km wide positive gravity anomaly of -165 mGal over the Abaya-Chamo rift, the 10 km wide negative gravity anomaly of -220 mGal over the Agereselam highland and ends at the -205 mGal gravity anomaly contour.

The transition of the crustal structure from one type to the other is clearly marked by steep gravity gradients (1.5 mGal/km for the western plateau-rift transition zone and 1.0 mGal/km for the eastern one). The Bouguer anomaly values increases from a minimum of -187 mGal on the Western Plateau to about -158 mGal over a 25 km wide zone at the centre of the rift and decreases from the later to about -222 mgal on the eastern plateau.

As mentioned earlier the average density of the whole upper mantle layer beneath the rift zone in East Africa is anomalously lower than that of a normal mantle of density 3.35 g/cm^3. It is determined to lie within the density interval estimated from the P-wave velocity /density conversion curves of Nafe-Drake, Birch and Henkel et al. (1990). The seismic

refraction results in Afar (Makris and Ginzburg, 1987) give a low velocity of 7.20 - 7.80 km/s for this anomalous mantle layer, suggesting a density interval of 3.00-3.20 g/cm^3. The lower limit of this density interval (3.00 g/cm^3) was used in modelling the anomalous mantle all throughout the model calculations.

Figure 10 shows the results of the computed model. The model demonstrates the following main tectonic features. Starting from the eastern edge of the Western Plateau, the crust is 40 km thick. It thins to 28 km over a distance of 35 km in the rift zone and thereafter increasing to 40 km at the western edge of the Eastern Plateau. The model consists of three crustal layers and two mantle layers: the top layer (sedimentary basin) consists of sediments and low density volcanics with its thickness varying from 2.5 to 5 km, the second layer (upper crust) with its thickness varying from 5 to 10 km, the third layer (lower crust) with its thickness varying from 14 to 29 km, the fourth layer (anomalous mantle) having a maximum thickness of 22 km and the normal mantle which lies at a depth of 50 km beneath the rift and 40 km beneath the plateaus.

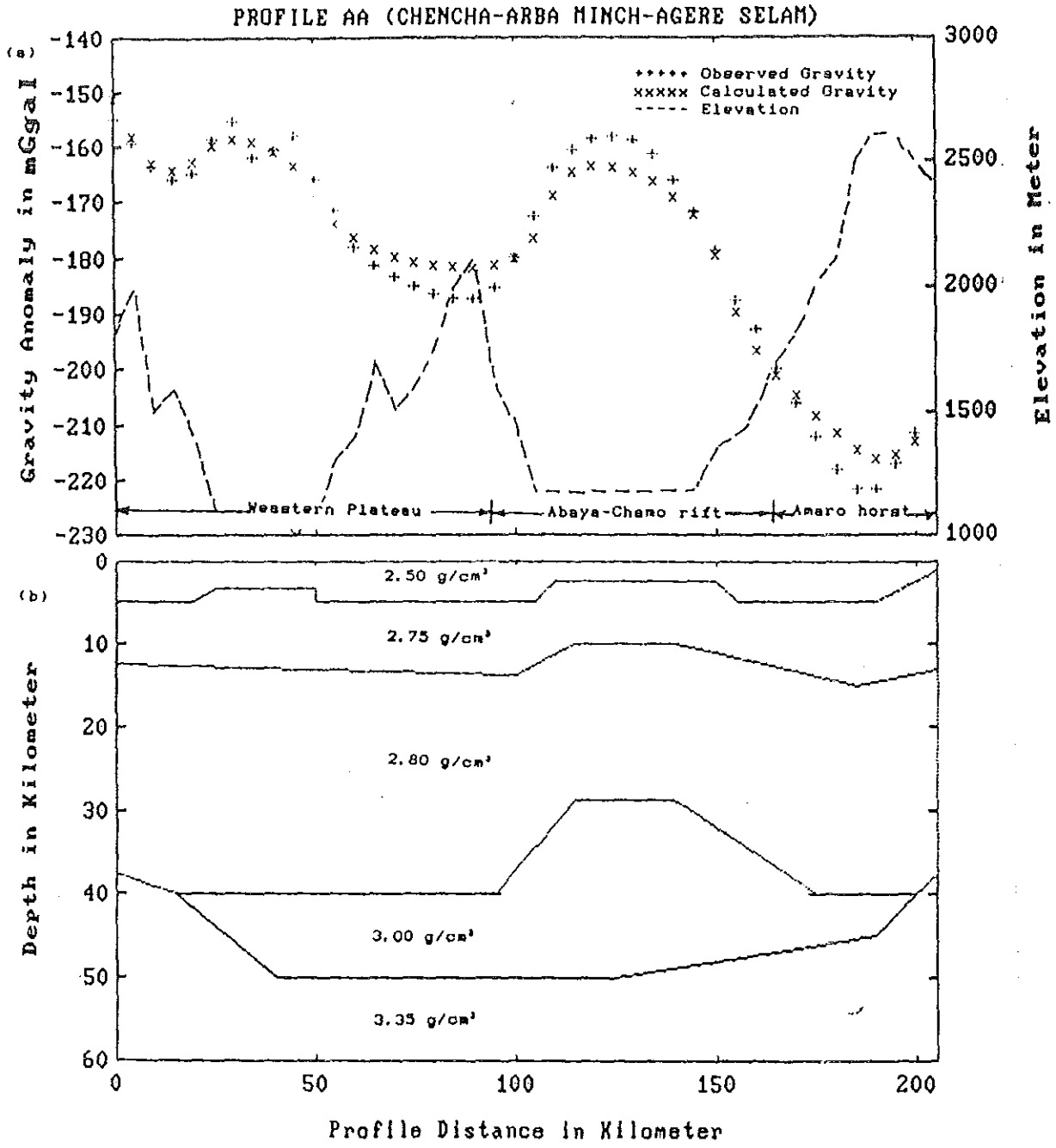

Fig. 10: (a) Gravity and the corresponding elevation profiles and (b) Crustal density model obtaind from gravity data constrained by seismic observations. The regional Bouguer anomaly trend along this profile decreases from the Western plateau to the Eastern plateau. The model shows that the crust beneath the rift is attenuated as compared to the normal crust beneath the plateaus due to the upward progression of the anomalous mantle to a shallow depth.

5.2.2 PROFILE BB (TURMI-CHEW BAHIR-KONSO-NEGELE)

This profile (Fig. 11) is 315 km long and starts from the western edge of the Hamer horst and crosses the Chew Bahir rift, the Boran-Konso horst, and the southern edge of the Amaro horst and then extends to the latitude of Negele. The profile thus crosses the major tectonic units (the horsts and the rift) in this region. A negative anomaly over the Chew Bahir Rift is flanked by relatively wide positive anomalies over the western and eastern highlands. The eastern positive anomaly gradually decreases to the east until it gets the minimum value about -181 mGal of the profile near the southern end of the Amaro Horst (Fig.7 & 11). The negative anomaly of width 48 km over this region is flanked by positive and negative anomalies to the east. The topography and the anomaly do not correlate over the Chew Bahir and the associated high lands, negative in the former and positive in the later. This is a completely different phenomena from the usual, i.e., the rifts such as the MER, the Afar depression, show positive anomalies while the highlands are associated with negative anomalies. The negative anomaly over the Chew Bahir rift is thought to be caused by thick accumulation of swamp and volcano lacustrine deposits of Pleistocene to present age (Fig. 3 & 7).

The Bouguer anomaly decreases from a maximum value about -74 mGal on the Hamer Horst to about -136 mGal over the centre of the Chew Bahir rift but the anomaly increases to the east to about -96 mGal over the Boran horst. East of the Boran horst

the anomaly decreases with a gradual slope 7.5 mGal/km to a minimum value of about -181 mGal and east of this it increases to -158 mGal after then the anomaly increases with a very gradual slope.

As in profile AA, the density values assigned to the sedimentary layer 2.5 g/cm^3, upper crust 2.75 g/cm^3, lower crust 2.80 g/cm^3, the anomalous mantel 3.0 g/cm^3 and the normal mantel 3.35 g/cm^3 are used throughout the model calculations. Figure 10 shows the results of the computed model. The model demonstrates the following main tectonic features. Starting from the eastern edge of the Hamer horst the thickness of the crust 27.5km continues constantly up to south of the Amaro Horst where it increases to 40 km. East of this region it thins to 35 km and again increase to 40 km towards the east.

As mentioned earlier the model consists of three crustal layers and two mantle layers: the top layer (sedimentary basin) consists of sediments and low density volcanics with its thickness varying from 1.25 to 7.5 km, the second layer (upper crust) with its thickness varying from 3.8 to 10 km, the third layer (lower crust) with its thickness varying from 15 to 30 km, the fourth layer (anomalous mantle) having a maximum thickness of 12.5 km and the normal mantle which lies at a depth of 50 km beneath the Chew Bahir rift and its flanking highlands (the Hamer and Boran horsts), 45 km beneath the southern edge of the Amaro Horst, and rising to 35 km beneath the eastern end of the profile.

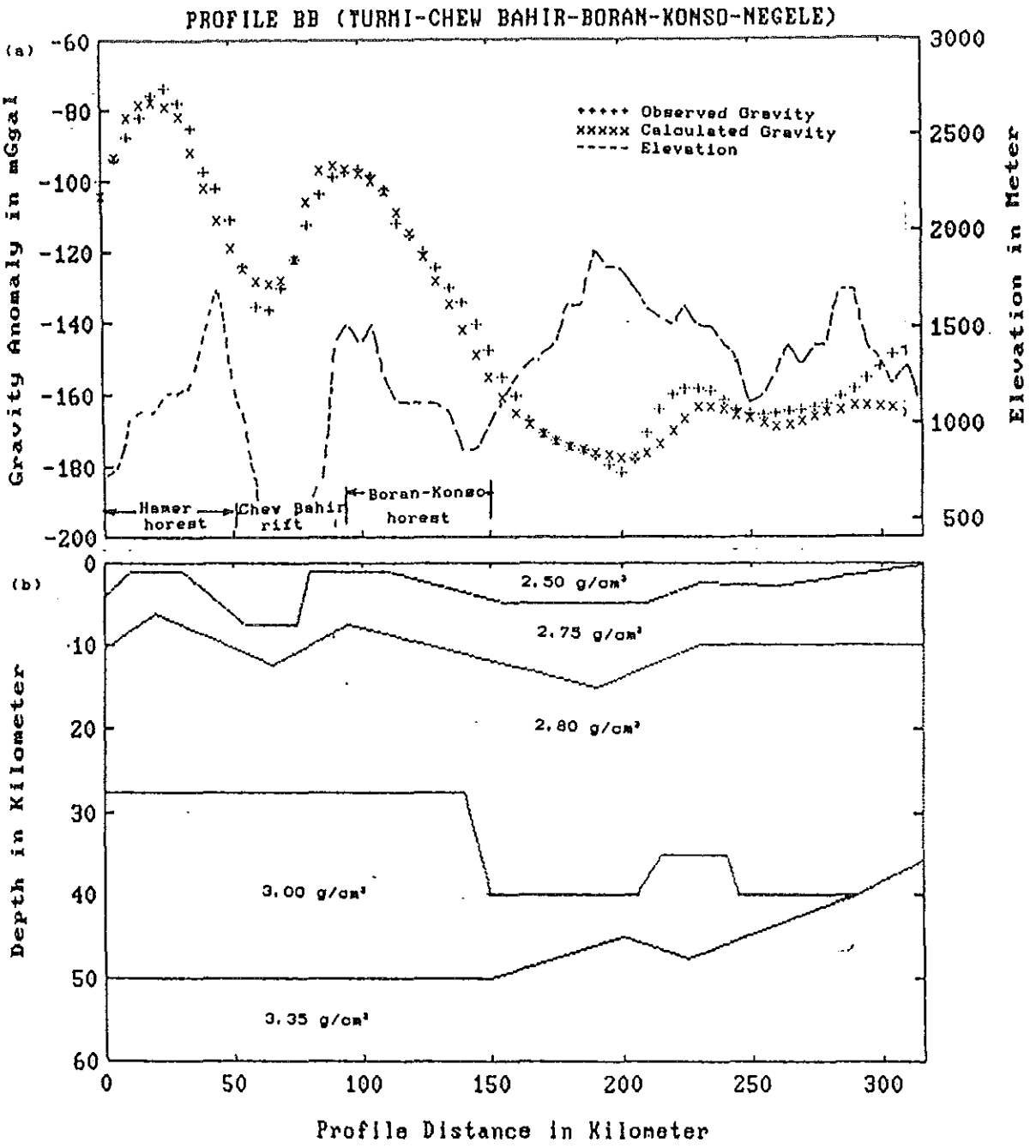

Fig. 11: (a) Gravity and the corresponding elevation profiles and (b) Crustal density model obtaind from gravity data constrained by seismic observations. The regional Bouguer anomaly trend along this profile decreases from the Western plateau to the Eastern plateau. The model shows that the crust beneath the Chew Bahir rift and its flanking high lands is attenuated due to the upward progression of the anomalous mantle to a depth of 27.5 km.

CHAPTER 6: DISCUSSIONS, CONCLUSIONS AND SUGGESTIONS

6.1 DISCUSSIONS

Before summarizing the results of this study thus far for the rift zone south of the southern end of the Main Ethiopian Rift, it is necessary to mention briefly what is known about the study area and its neighbouring regions.

No refraction seismic information is available concerning the crustal structure of the study area. It is known that the Turkana rift is underlain by an anomalous upper mantle with a velocity of 7.48 km/s from the refraction seismic experiment of Griffiths (1972). Along this profile the lower crust is penetrated by a narrow belt of anomalous mantle to a depth of 20 to 22 km.

Further south in the Kenyan Rift the anomalous mantle is mapped at a depth of 35 km (KRISP85 experiment results). These results demonstrate a thickening of the crust along the rift axis towards the Kenyan dome. Further north of the study area along the rift axis in Ethiopia, the 2½-D gravity models computed by Alemu (1992) indicate that the crust thickens to 30 km in the central part of the MER. The thickening is consistent with the regional gravity data.

Gravity values generally decrease from about -100 mGal from around southern Turkana to about -200 mGal near Lake Naivasha

(centre of Kenyan dome) southwards along the Kenyan rift and to about -195 mGal in the central part of the MER (at about latitude 7^0N) along the rift axis in Ethiopia (Alemu, 1992).

Seismicity studies beneath the rift zones in East Africa confirm that most earthquake activities occur within the rift system, indicating that this fault system is still developing. The seismically active zones are marked by cluster of earthquake epicentres, recent volcanic activities, steep gravity gradients and local positive gravity anomalies.

The earthquake history of the study area indicates that in the region between 4^0N and 6^0N, there has been a significant number of earthquake activities with magnitude between 5 and 6.5 associated with rifting (Asfaw, 1990).

Looking at Figure 7, the positive anomalies lie over the rift zones in the study area. The anomaly increases positively from north to south, indicating the thinning of the lower crust in the same direction. The locations of alternating bands of negative and positive anomalies coincide with the locations of crustal attenuations associated with rifting. From the computed models, we can see that the crust has a thickness of 27km below the Chew Bahir Rift and the flanking uplifted regions. This shows that the Chew Bahir rift zone is intermediate to the Turkana Rift and the MER regarding crustal thinning.

From the foregoing analysis of the gravity data, the prominent

point that can be highlighted is the correlation between the pattern of the gravity anomalies associated with the Abaya-Chamo rift and the flanking plateaus and those of the Chew Bahir Rift and its flanking high lands (Fig. 7 & 2). It has been observed that a positive anomaly is associated with the Abaya-Chamo rift floor and a negative anomaly with its flanking uplifted regions. This is a superposition of a narrow positive anomaly on a larger negative one. The gravity survey described for the northern extension of the MER (Alemu, 1992; Alemu & Sjöberg, 1990), the Afar depression (Makris et al., 1972), the Gregory rift (Searle, 1970) has shown this pattern (superposition of a positive anomaly on a large negative one) is a typical characteristics of the gravity field of the East African rift system. In general, the axis of the positive anomaly corresponds to the axis of the rift.

On the contrary, a negative anomaly is associated with the floor of the Chew Bahir rift and a positive anomaly with its flanking uplifted regions (Hamer, Boran-Konso horsts), i.e., a superposition of a negative anomaly over a large positive one. The anomaly pattern here is completely different from that of the Abaya-Chamo rift. Unlike the MER and the Gregory rift, axial positive anomaly is not observed over the Chew Bahir rift. This is infact a new phenomena discovered in this research when compared to the anomaly pattern exhibited by the other segments of the East African rift system. The negative anomaly over the Chew Bahir rift is thought to be caused by thick accumulation of swamp and Volcano lacustrine sediments

since Pleistocene to present.

6.2 CONCLUSIONS AND SUGGESTIONS

The gravity data presented will play an important role in an interdisciplinary interpretation, in which all available geoscientific information of recent and future work in the Ethiopian Rift system are gathered.

The crustal structure of the study area has been interpreted using the seismic refraction profiles obtained for the rift zone in Ethiopia and Kenya, the existing geological and seismicity information of the region and constraints generated from the new Bouguer anomaly map constructed for this purpose.

The main conclusions of this study are:

The measured gravity field for the study area seems to be a sensitive indicator of the tectonic and geologic structures in the region. The crustal models computed for the selected profiles (Fig. 10 & 11) indicate that the lower crust has been replaced by a zone of denser material (anomalous mantle) beneath the rift zones.

The Chew Bahir Rift and its flanking uplifted lands (Fig. 11) show a completely different anomaly picture from those of the neighbouring rift segments, i.e., a negative anomaly over the rift floor, which is thought to be caused by thick accumulation

of swamp and Volcano lacustrine sediments since Pleistocene to present, and positive anomalies over the associated high lands are observed. East of the southern edge of the Amaro horst (Fig. 11) the anomalous mantle rises to a height of 5 km above the crust-mantle boundary.

In view of these conclusions the following suggestions for further work are made:

Without doubt further refinements of the observations, and consequently of the interpretations, can be made. In particular terrain corrections, the dominating error source to Δg in this study, should be added.

Additional geophysical work such as refraction seismic, together with more detailed studies of the gravity field and density determinations of the rocks flooring the area will provide better data for quantitative interpretations.

Detailed seismic studies of this region will provide a valuable data for a further analysis of the crustal structure beneath it.

REFERENCES

Alemu, A., 1983. Crustal Modelling from Gravity Data in the Ethiopian Rift. M.Sc. Thesis, Addis Ababa University, Addis Ababa, Ethiopia. (unpublished).

Alemu, A. 1988. Gravity Field Interpretation Over the Main Ethiopian Rift. Proceedings of the 6th International Symposium "Geodesy and Physics of the Earth", Potsdam, Part II, pp. 99-115.

Alemu, A., 1992. The Gravity Field and Crustal Structure of the Main Ethiopian Rift. Ph.D. Thesis, Royal Institute of Technology, Department of Geodesy, Report No. 26 (TRITA GEOD 1026), Stockholm, Sweden.

Alemu, A., Sjöberg, L.E., 1990. Gravity Field Interpretation and Crustal Model Studies in the Main Ethiopian Rift. Presented at the Third International Symposium on Recent Crustal Movements in Africa. 8-16 December 1990, Aswan, Egypt.

Asfaw, L.M., 1990. Implication of shear deformation and earthquake distribution in the East African Rift between 4^0N and 6^0N. Journal of African Earth Sciences, 10: (4) 745-751.

Baker, B.H, Mohr, P.A. and Williams, L.A.J., 1972. Geology of the East Rift System of Africa. Geol. Soc. Am., Spec. Pap., 136:67pp.

Barberi, F., Borsi, S., Ferrara, G., Marinelli, G., and Varet, J., 1970. Relationships between tectonics and magmatology of the northern Afar (Danakil) depression: Royal Soc. London philos. Trans., Ser. A, v. 267, p. 293-311.

Birch, F., 1961. The velocity of compressional waves in rocks to 10 kilobars. Part II: Journal of Geophysical research; vol. 66; pp. 2199-2223

Bjerhammar, A., 1973. Theory of errors and generalized matrix inverses. Elsevier Scientific Publishing Company, Amsterdam

Comucci, P., 1950. Le vulcaniti del Lago Tana (Africa Orientale): Accad. Naz. Lincei, Roma, 209 p

Davidson, A., compiler, 1983. The Omo River project, reconnaissance geology and geochemistry of parts of Ilubabor, Kefa, Gemu Gofa and Sidamo: Minstry of Mines and Energy,Ethiopian Institute of Geological Surveys, Bulletin No. 2, p. 1-89.

De Heinzelin, J., Brown, F.J. and Howell, F.C., 1971. Pliocene/pleistocene formations in the Lower Omo Basin, southern Ethiopia. Quaternaria, 13: 247-268.

Ebinger, C., 1991. Southern Ethiopia Rift Gravity surveys: Interim Report to the Ethiopian Institute of Geological Surveys. Leeds University Dept. of Earth Sciences.

Falcon, N.L., Gass, I.G, Girdler, R.W. and Laughton, A.S.(Editors), 1970. A discussion on the structures and evolution of the Red Sea , Gulf of Aden and Ethiopian rift junction. Phil. Trans. R. Soc. London, Ser. A, 267: 1-417.

Garland, G.D., 1979. Introduction to Geophysics - Mantle, Core and Crust, W.B Saunders Company, Philadelphia.

Gibson, I., L., 1967. Preliminary account of the volcanic geology of Fantale, shoa: Bull. Geophys. obs. Addis Ababa, no. 10, p. 59-67.

Gibson, I., L., 1970. Quaternary panteleritic volcanism in the main Ethiopian rift: univ.Leeds, Dept. Earth sci., 14th Ann. Rept. Research Inst. Africa Geol., p. 35-38.

Girdler, R.W., Fairhead, J.D., Searle, R.C. and Sowerbutts, W.T.C., 1969. The Evolution of Rifting in Africa, Nature, 224: 1178-1182.

Griffiths, D. H., 1972: Some comments on the results of a seismic refraction experiment in the Kenya rift; Tectonophysics, vol. 15, pp 151-156.

Heiskanen, W.A. and Moritz, H., 1967. Physical Geodesy, Freeman, San Francisco.

Henkel, H., Lee, M.K., Lund, C-E. and Rasmussen, T. 1990. An

integrated geophysical interpretation of the 2000 km Fennolora section of the Baltic shield. Geological Survey of Sweden, Uppsala.

Herbert, L. and Langston, C. A., 1985. Crustal thickness estimates at AAE (Addis Ababa, Ethiopia) and NAI (Nairobi, Kenya) using P-Wave conversions. Tectonophysics, 111, 299-327.

Jepsen, D.H., and Athearn, M.J., 1961. General geology map of the Blue Nile basin, Ethiopia (1:1 million): U.S. Dept. of state, Washington, D.C

Kazmin, V., 1972. Geological map of Ethiopia. Ethiopian Geological Survey Ministry of Mines, Addis Ababa Ethiopia.

Khan, M. A. and KRISP working group, 1987. Structure of the Kenyan Rift from seismic refraction (KRISP). Nature, 325: 239-242.

Keller, G.R., Braile, L.W., Davis, P.M., Meyer, R.P., Mooney, W.D., and the KRISP Working Group, 1992. KRISP, 1989-1990 Experiment, Eos, Vol.73. no.33, pp. 345, 349-351.

LeBas, M. J., and Mohr, P. A., 1968. Feldspathoidal rocks from the cenozoic volcanic province of Ethiopia: Geol. Rundschau, v. 58, p. 273-280.

Levitte,D., Coulomba, C. and Mohr, P. 1974. Reconnaissance

geology of the Amaro Horst, Southern Ethiopian Rift. Geol. Soc. Am. Bull. 85, 417 - 422.

Makris, J., Menzel, H., and Zimmermann, J., 1972. A preliminary interpretation of the gravity field of Afar, northeast Ethiopia. In: R.W. Girdler (editor), East African Rifts. Tectonophysics 15 (1/2), 31-39.

Makris, J., Menzel, H., Zimmermann, J. and Gouin, P., 1975. Gravity Field and Crustal Structure of North Ethiopia. In: A. Pilger and A. Rösler (editors), Afar depression of Ethiopia. Stuttgart (Schweizerbart), 1: 135-144.

Makris, J. and Ginzburg, A., 1987. The Afar Depression: Transition between continental rifting and sea floor spreading. Tectonophysics, 141: 199 - 214.

Marsden, G. Southern Ethiopian Rift Gravity Surveys. (unpublished)

Merla, G., Abbate, E., Canuti, P., Sagri, M., and Tacconi, P., 1973. Geological Map of Ethiopia and Somalia, scale 1:2,000,000: Firenze, Italy.

Mohr, P.A., 1960. Report on a geological excursion through southern Ethiopia: Bull. Geophys. obs. Addis Ababa, no. 3, p. 9-20.

Mohr, P.A., 1962. Surface cauldron subsidence with associated faulting and fissure basalt eruptions at Gariboldi pass, shoa Ethiopia: Bull. volcanol., v. 24, p. 421-428.

Mohr, P.A., 1966. Chabbi Volcano (Ethiopia) Bull. Volcan. 29:797-816

Mohr, P.A., 1967a. The Ethiopian rift system: Bull. Geophys. Obs. Addis Ababa, no. 11, p. 1-65.

Mohr, P.A., 1967b. Review of the geology of the simien Mountains: Bull. Geophys. Obs. Addis Ababa, no.10, p. 79-93.

Mohr, P.A., 1967c. Major volcano-Tectonic lineament in the Ethiopian rift system: Nature, v. 213, p. 664-665.

Mohr, P.A., 1968. The cenozoic volcanic succession in Ethiopia: Bull. volcanol., v.32, p. 5-14.

Mohr, P.A., 1971a. The Geology of Ethiopia: Haile Sellassie I university press, p. 161-164.

Mohr, P.A., 1971b. Tectonics of the Dobi graben region, Central Afar, Ethiopia. Bull. Geophys. Obs. Addis Ababa, 13: 73-89.

Mohr, P.A., 1987: Structural style of the continental Rifting in Ethiopia: Reverse collements, EOS, Vol. 68, no. 35, pp. 721, 729-730.

Mohr, P.A and Wood, C.A., 1976. Volcano spacings and lithospheric attenuation in the Eastern Rift of Africa. Earth Planet. Sci. Lett. 33: 126-144.

Moore, Jr., J.M. and Davidson, A.,1978. Rift structure in southern Ethiopia. Tectonophysics, 46: 159-173.

Mortiz, H., 1971. Geodetic References System 1967. Pub. No.3, Bulletin Geodesique, Paris.

Nafe, I., E.; Drake, C. L., 1963. Physical properties of marine sediments; Hill (editor) The Sea; Interscience, 794-815.

Rasmussen, R. and Pederson L. B., 1979. End corrections in potential field modelling, Geophysical Prospecting 27, 749-760.

Searle, R.C., 1970. Evidence of Gravity Anomalies for the Thinning of the Lithosphere Beneath the Rift Valley in Kenya. Geophys. Journal Roy. Astron. Society. 21: 13-31.

Searle, R.C and Gouin, P., 1972. A Gravity Survey of the Central Part of the Ethiopian Rift Valley. Tectonophysics. 15: 41-52.

Sjöberg, L. E., 1990. The best linear combinations of L1 and L2 frequency observables in the application of Transit/Doppler and GPS. Manuscripta geodaetica 15: 17-22.

Sjöberg, L.E., 1990. Physical Geodesy. Royal Institute of Technology, Department of Geodesy, (TRITA GEOD 2009), Stockholm, Sweden.

Swain, C.J. and Khan, M.A., 1977. A Catalogue of Gravity Measurements. Geology Dept., Leicester University.

Talwani, M., 1973. Computer usage in the computation of gravity anomalies, in computational physics, ed. by B. Alder, vol. 13, 343-389.

Talwani, M., Worzel, J.L. and Landisman, M., 1959. Rapid Gravity Computations for Two-Dimensional Bodies with an Application to the Mendocino Submarine Fracture zone. J. G.R., 64: 49-59.

Tazieff, H. and Varet, J., 1969. Signification tectonique et magmatique de L'Afar septentrional (Ethiopie). Rev. Geographie Phys. et Geologie Dynam., vol. 11, pp. 429-450.

Telford, W.M., Sheriff, R.E., and Geldart, L.P. 1990. Applied Geophysics, 2nd ed. Cambridge: Cambridge University Press.

Tsuboi, C., 1983. Gravity. George allen and Unwin (publishers) Ltd. U.K.

Wolde Gabriel, G., and Aronson, J.I., 1987. Chow Bahir rift: A " failed" rift in Southern Ethiopia: Geology, v. 15 p. 430-433.

Wolde, B., 1989. Cenozoic volcanism and rift development in Ethiopia. Journal of African Earth Sciences, vol.8, No.1,pp.99-105.

Woolard, G.P., 1959. Crustal structure from Gravity and Seismic Measurements. Journal of Geophysical research; vol. 64; no.10; pp. 1521-1544.

Zanettin, B., Justin - Visentin, E., Nicoletti, M. and Petrucciani C. 1978. The evolution of the Chencha escarpment and the Ganjuli graben (Lake Abaya) in the southern Ethiopian rift. N. Jb. Geol. Palaont. 8, 473-490